NAWI Graz
Natural Sciences

TU Graz

Walter Ladreiter, BSc

Startup and Shutdown Strategies with Oxygen Consumption for Polymer Electrolyte Fuel Cells

MASTER'S THESIS

to achieve the university degree of

Diplom-Ingenieur

Master's degree programme: Technical Chemistry

submitted to

Graz University of Technology

Supervisors

Assoc.Prof. Dipl.-Ing. Dr.techn. Viktor Hacker

Dipl.-Ing. Katharina Kocher, BSc

Institute of Chemical Engineering and Environmental Technology

Faculty of Technical Chemistry, Chemical and Process Engineering and Biotechnology

Graz, July 2020

Affidavit

I declare that I have authored this thesis independently, that I have not used other than the declared sources/resources, and that I have explicitly marked all material, which has been quoted either literally or by content from the sources used. The text document uploaded on TUGRAZonline is identically to the present master's thesis.

Ich erkläre an Eides statt, dass ich die vorliegende Arbeit selbstständig verfasst, andere als die angegebenen Quellen/Hilfsmittel nicht benutzt, und die den benutzten Quellen wörtlich und inhaltlich entnommenen Stellen als solche kenntlich gemacht habe. Das in TUGRAZonline hochgeladene Textdokument ist mit der vorliegenden Masterarbeit identisch.

_____   _____
              Date   Signature

Acknowledgements

First of all, I want to thank Assoc. Prof. Viktor Hacker for the supervision of my master's thesis as well as for the opportunity to join the fuel cells working group. At this point I also want to express gratitude for the opportunity to continue my work within the working group beyond the scope of this thesis.

I want to thank Katharina Kocher for the supervision and for her extensive support and advise during all the different stages of my master's thesis.

Special thanks go to Dinilesizwe Ndayi and Christoph Schuetz from Greenlight Innovation GmbH, for their experienced technical support provided for many times, and also to Bernhard Marius, for sharing a lot of knowledge on fuel cell testing and how to operate and maintain test stations, which has proven to be essential during my practical work.

Further, I want to thank the entire fuel cells working group for many advices, shared experiences and ideas, and also for the friendly working atmosphere. I am very glad to be able to continue working with you in the future.

Last, but not least, I want to thank my family and my friends accompanying and supporting me during my time studying here in Graz. Especially, I want to thank my parents for always supporting me morally as well as financially, without ever putting me under pressure.

Kurzfassung

Diese Arbeit befasst sich mit der Erhöhung der Lebensdauer von Polymerelektrolytbrennstoffzellen (PEFC) unter den dynamischen Betriebsbedingungen von Transportanwendungen. Beim Einsatz in Brennstoffzellenfahrzeugen sind vor allem Vorgänge während des Starts/Stopps (SUSD) der Zellen Hauptursache für Degradations-erscheinungen. Dabei treten Wasserstoff/Sauerstoff-Fronten an der Anode auf, welche die lokale Spannung nahezu auf das Doppelte der Leerlaufspannung erhöhen. Dies führt zu verschiedenen Schädigungen, wobei die Kohlenstoffkorrosion am Katalysatorträger die stärkste Verringerung der Lebensdauer mit sich bringt. Eine vielversprechende Möglichkeit, diesem Problem zu begegnen, ohne auf neue Materialien oder Zellkomponenten zurückgreifen zu müssen, ist die Anwendung von SUSD-Strategien, um diese schädlichen Betriebsbedingungen zu vermeiden. Im Zuge dieser Arbeit wird eine SUSD-Strategie getestet, in welcher beim Stopp der Zelle der Sauerstoff vollständig verbraucht wird, um die Degradation der Zelle zu vermeiden.

Basierend auf dieser Referenzstrategie werden zwei weitere Strategien entwickelt. Die erste davon zielt darauf ab, den durch hohe Leerlaufspannungen bedingten Leistungsverlust zu minimieren. In der zweiten Variante werden Schäden durch Wasserstoffmangel bei schnellen Lastwechseln reduziert, indem die elektrische Last bei Start und Stopp stufenweise erhöht bzw. verringert wird. Diese drei Strategien werden mit einer vierten verglichen, welche die Ausbildung von H_2/O_2-Fronten beinhaltet. Dazu wird die Anode während des Herunterfahrens mit Luft gespült. Die Charakterisierung der Testzellen umfasst die Aufnahme von Polarisationskurven, Zyklovoltammetrie, Lineare Sweep Voltammetrie und elektrochemische Impedanzspektroskopie. Weiters werden die CO_2- und CO-Gehalte im Kathodenabgas analysiert, um die Degradationen durch Kohlenstoffkorrosion zu quantifizieren. Die Ergebnisse zeigen, dass das Vermeiden der H_2/O_2-Fronten signifikante Vorteile mit sich bringt. Alle drei entsprechenden Strategien führten im Vergleich zur vierten Strategie zu weniger Leistungsverlusten und Kohlenstoffkorrosion, wobei die beiden Variationen der Referenzstrategie keine Verbesserungen, sondern leichte Verschlechterungen zur Folge hatten.

Abstract

This thesis aims to enhance the lifetime of polymer electrolyte fuel cells (PEFC) under the dynamic conditions of transport applications. In fuel cell electric vehicles (FCEV), startup and shutdown (SUSD) of the cell are major sources of degradation. During SUSD, H_2/O_2 boundaries occur in the anode compartment, elevating the cell potential to almost twice the open circuit voltage (OCV). This leads to various types of damage, with carbon corrosion on the catalyst support causing the greatest reduction in service life. A promising strategy to cope with this issue, without the need of new materials for cell components, is to introduce SUSD strategies avoiding or extensively mitigating degradation effects. In this thesis, a SUSD strategy is tested where oxygen is completely consumed during shutdown to avoid PEFC degradation. Based on this reference strategy, two additional variants are created. The first one aims to avoid performance decay related to open circuit voltage conditions. In the second, damage caused by hydrogen deficiency during rapid load changes is reduced by gradually increasing or decreasing the electrical load during start and stop. These three strategies are compared with a SUSD strategy featuring the formation of H_2/O_2 boundaries, this is done by purging the anode with air to remove H_2 during shutdown.

The characterization of test cells includes the recording of polarization curves, cyclic voltammetry, linear sweep voltammetry and electrochemical impedance spectroscopy. In addition, carbon dioxide and carbon monoxide contents in the cathode off gas are analysed to quantify degradation caused by carbon corrosion.

The results show that avoiding H_2/O_2 fronts has significant advantages regarding PEFC durability. All three O_2 consumption SUSD strategies lead to less power losses and carbon corrosion compared to the fourth strategy with anode air purge.

Contents

1.   Introduction

In 2019, Oxford Dictionaries has declared the expression "climate emergency" to the word of the year [1]. The public awareness of anthropogenic climate change is growing, public media and politics increasingly set their focus on topics regarding climate and environment. Meanwhile, the annual global greenhouse gas (GHG) emissions caused by humanity have rather grown. Between 2013 and 2016, each year around 32 gigatons of carbon dioxide (CO_2) emissions were caused by the combustion of fossil fuels. After this short period of stability, in 2017 there has been another gain of 1.5%, mostly caused by growing industries. At the United Nations Climate Change Conference in 2015, the contributing parties agreed to keep the global temperature increase below 2 °C and take further efforts to limit it to a maximum of 1.5 °C above pre-industrial levels [2]. Reaching those goals will require a significant decrease in the use of fossil fuels, causing challenging scientific and economic issues, especially in the transport sector. Since more than a quarter of the total GHG emissions originates there, it will be necessary to reduce the mass of individual road traffic by shifting towards more public transport, and replace internal combustion engines by environmentally friendly alternatives.

The most promising alternative to internal combustion engine vehicles (ICEVs) are electric vehicles (EVs). They do not emit greenhouse gases while driving, true zero emission operation can be reached if the current is supplied by CO_2-neutral power sources. Using an electric motor instead of an internal combustion engine provides even more benefits. Compared to latter, they are much simpler and more efficient, they run smooth, relatively silent and produce high torque over their whole speed range, hence no complex transmission is needed. The main challenge coming up with EVs is the choice of an adequate power supply. In recent years, battery electric vehicles (BEVs) featuring lithium ion batteries became fastest spreading option. They are highly efficient and suitable for most individual traffic scenarios. However batteries are less beneficial for big vehicles or if high ranges are demanded. Batteries take a big share of an BEV's costs, and more range means larger batteries are required. Increasing the range extraordinarily rises the price and the need of precious resources, but simultaneously decreases efficiency due to high weight [3].

Another option of power supply for EVs are hydrogen fuel cells. Fuel cell electric vehicles (FCEVs) also operate silent and have no emissions except of water. Fuel cells might not be able to compete with batteries in short distance applications due to their relatively high costs and lower efficiency, but they offer great potential for applications where batteries struggle. The range of FCEVs is determined by the size of the hydrogen storage tank, therefore higher ranges are easy to achieve without excessive negative impacts on costs and efficiency. Also, refueling a hydrogen storage takes much less time than recharging a battery. This makes fuel cells a good option for long range transport, but also for applications where long operation times are needed, such as machines used in agriculture, construction or mining. For automotive applications, polymer electrolyte fuel cells (PEFC) represent the most promising type [4].

However, PEFC technology itself has some challenges left that have to be faced. One of the biggest remaining issues is FC durability. PEFCs may constantly operate for several ten thousand of hours, but the 5000 hours target set by the US Department of Energy has not been reached yet [5]. Practical operation conditions for automotive PEFCs are dynamic. Beside high power, idling and load changes, start up and shutdown (SUSD) lead to significant degradation of a cell's key components. Although the introduction of catalyst support materials less susceptible to corrosion and the optimization of catalyst behavior are considered promising, these solutions are still under development and yet not available for widespread practical application. Therefore, a comparatively low cost alternative is to reduce degradation by optimizing operation parameters.

In this context, the aim of this work is to compare the performance behavior of a single PEFC operated with different SUSD strategies and characterize their degradation potential. The main focus lays on avoiding hydrogen/air fronts in the cell, which are known to be the main cause of FC degradation during start/stop operation. Each strategy is tested by applying a certain number of SUSD cycles, after which the cell is electrochemically characterized in-situ by polarization curves (UI), cyclic voltammetry (CV), linear sweep voltammetry (LSV) and electrochemical impedance spectroscopy (EIS). In addition, CO_2 and CO contents in the cathode off-gas are measured to quantify carbon corrosion during SUSD.

2. Theory

2.1. Fuel cell basics

A fuel cell is a galvanic cell capable of producing electric current from the reaction of a fuel and an oxidant. Most fuel cell systems use hydrogen as fuel, it is reacted either with air or with pure oxygen. The direct combustion of hydrogen with oxygen is an uncontrolled reaction in which high amounts of heat are set free. The fuel's chemical energy is converted to heat. In contrast to this warm combustion, the controlled "cold combustion" taking place in a fuel cell shows no flame, the chemical energy of the hydrogen molecules is converted directly into electrical energy, only low amounts of heat generated.

Like any electrochemical element, a fuel cell roughly consists of two electrodes separated by an electrolyte. Based on the materials the electrodes and electrolyte are made of, several types of fuel cells can be distinguished. Because of its high power density and low operation temperature, the most common and currently most promising fuel cell type is the polymer electrolyte fuel cell (PEFC) [6]. The working principle of a PEFC is shown in 1.
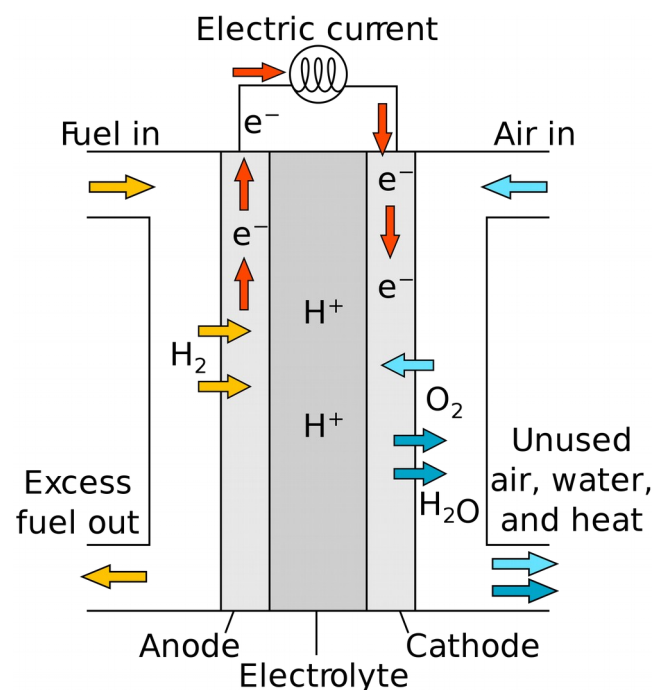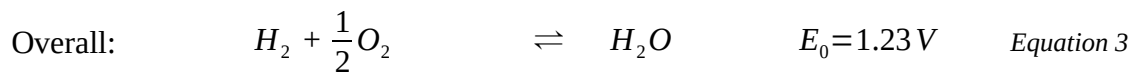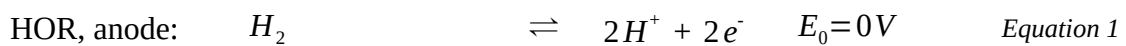

Figure 1: Working principle of a proton exchange membrane fuel cell, depicted from [7]

On the negative electrode, the anode, hydrogen is oxidized. The protons are able to permeate through the ion conducting electrolyte membrane. The hydrogen oxidation reaction (HOR), is shown in Equation 1. The electrons, due to the membrane's electrically insulating behavior, are transferred via an external electric circuit, resulting in an electric current. At the positive electrode, the cathode, those electrons, along with the protons and oxygen molecules, take part in the oxygen reduction reaction (Equation 2), forming water as exhaust product.

HOR, anode:	H_2	$\rightleftharpoons \quad 2H^+ + 2e^-$	$E_0 = 0\,V$	*Equation 1*
ORR, cathode:	$\frac{1}{2}O_2 + 2H^+ + 2e^-$	$\rightleftharpoons \quad H_2O$	$E_0 = 1.23\,V$	*Equation 2*
Overall:	$H_2 + \frac{1}{2}O_2$	$\rightleftharpoons \quad H_2O$	$E_0 = 1.23\,V$	*Equation 3*

The overall reaction shown in Equation 3 is equal to the reaction of hydrogen combustion [8]. The heat, or enthalpy (ΔH) released in this exothermic reaction equates the difference between the standard enthalpy of formation (h_f) of the product (H_2O) and the reactants (H_2 and O_2):

$$\Delta H = (h_f)_{H_2O} - (h_f)_{H_2} - \frac{1}{2}(h_f)_{O_2} \qquad \textit{Equation 4}$$

The reaction enthalpy ΔH can be seen as the maximum energy that can be withdrawn from H_2. Obeying the laws of thermodynamic, FCs can obviously never convert the full amount of reaction enthalpy into electrical energy. The convertible amount of energy is known as Gibbs free energy (ΔG) and can be calculated with the following equation, where T is the temperature and ΔS the change of entropy.

$$\Delta G = \Delta H - T\,\Delta S \qquad \textit{Equation 5}$$

The change in entropy (ΔS) is equal to the difference between the standard entropy of formation of the product (H_2O) and the reactants (H_2 and O_2):

$$\Delta S = (s_f)_{H_2O} - (s_f)_{H_2} - \frac{1}{2}(s_f)_{O_2} \qquad \textit{Equation 6}$$

The resulting change in entropy is -0.1633 kJ mol^{-1} K^{-1}, at 25 °C (298 K), using the HHV, this gives a Gibbs free energy of -237.3 kJ mol^{-1}. This is the maximum amount of energy which can be converted, the remaining 48.7 kJ mol^{-1} are released as heat. ΔG divided by ΔH results in the fuel cell's ideal efficiency:

$$\eta_{ideal} = \frac{\Delta G}{\Delta H} = 83\%$$
Equation 7

The relationship between ΔG and the reversible cell potential (E$_0$) is shown in the following equation, with z being the number of transferred electrons per hydrogen molecule and F the Faraday constant:

$$E_0 = \frac{-\Delta G}{z\,F} = \frac{237.3\,kJ\,mol^{-1}}{2*96485\,C\,mol^{-1}} = 1.23\,V$$
Equation 8

The ideal efficiency as well as the reversible cell potential are theoretical values which are not reached in practical fuel cell operation. There are voltage losses caused by factors like electrical/ionic resistance of cell components, fuel crossover, reactants transport, internal currents and reaction kinetics [9]. The practical efficiency can be calculated by multiplying the ideal efficiency with the potential efficiency [10], shown in the following equation:

$$\eta_{practical} = \eta_{ideal} * \eta_E = \frac{\Delta G}{\Delta H} * \frac{E_{real}}{E_0}$$
Equation 9

A fuel cell's potential is also influenced by the temperature and the partial pressures of the reactants and the product. The combination of Equation 5 and Equation 8 gives the relationship between E and T (Equation 10). Since ΔS is negative, the cell potential is expected to decrease with raising temperature. However, since voltage losses are lower at higher T, the real potential increases instead [8].

$$E_0 = -\frac{\Delta H - T\Delta S}{z\,F}$$
Equation 10

The pressure dependence of the cell potential can be expressed with Nernst's equation, where R is the ideal gas constant (8.31446 J mol^{-1} K^{-1}) and p the partial pressure:

$$E = E_0 + \frac{R*T}{z*F} \ln\left(\frac{p_{H_2} * p_{O_2}^{0.5}}{p_{H_2O}}\right)$$
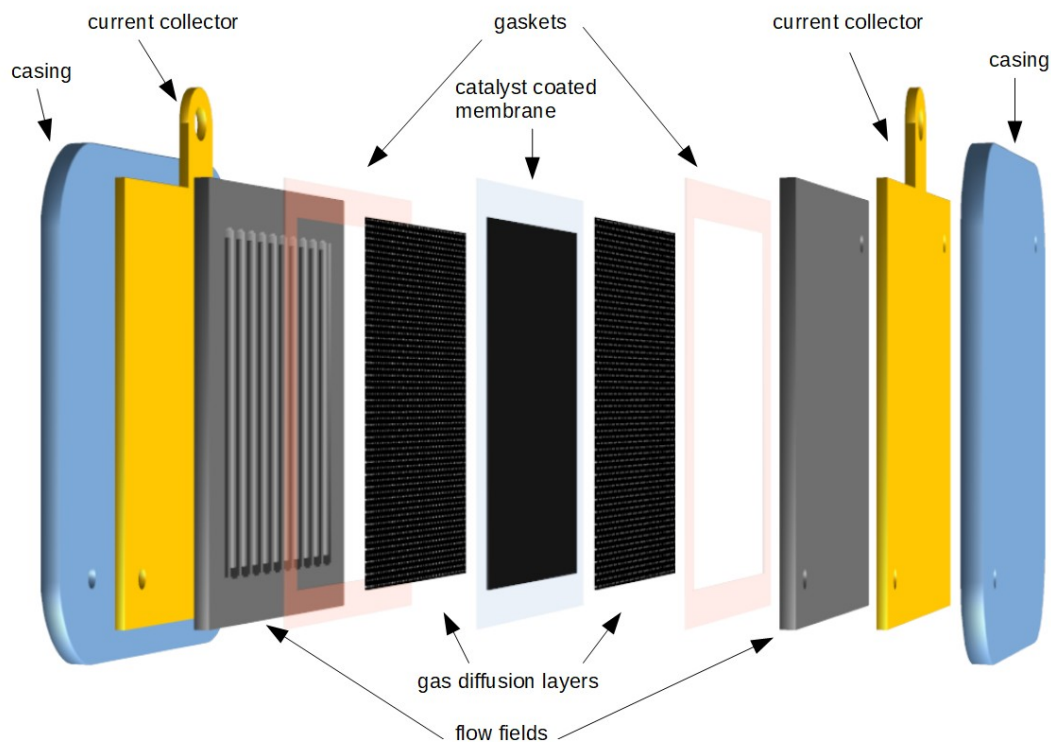
Equation 11

2.2. PEFC components

Figure 2: Explosion view of a typical PEFC

A schematic view of the components of a typical single PEFC is shown in 2. The **catalyst-coated membrane (CCM)**, where the electrochemical reactions take place, is the "heart" of the fuel cell. The membrane has to exhibit a high proton conductivity while being an electrical insulator and impermeable for reactant gases. Copolymers of tetrafluorethylene and perfluorosulfonates are the materials best meeting those demands. The best known one, Nafion™ (developed by DuPont) is shown in 3.
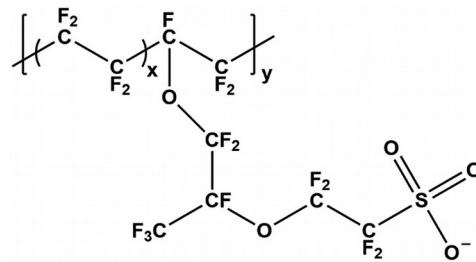
Figure 3: Structure of Nafion^{TM}, depicted from [11]

In order to enable proton conductivity, the presence of water is needed, so the reactant gases need to be humidified. The membrane can uptake a reasonable amount of water, causing the formation of proton conducting clusters and channels, as shown in 4. Solvated protons are able to migrate through the membrane by traveling between neighboring sulfonate groups . Generally, the conductivity increases with temperature, nevertheless the membrane temperature should not exceed 90 °C, since this may cause the destruction of the sulfonate groups and alter the polymer morphology [12].
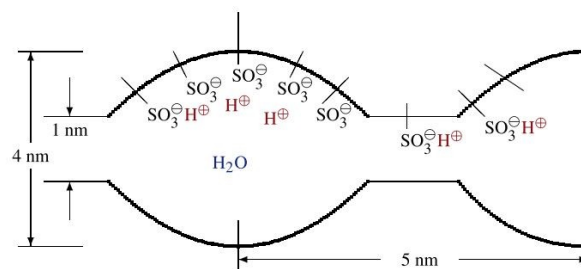

Figure 4: Principle of H+ conductivity of Nafion^{TM}, depicted from [4]

The membrane is coated with a thin layer of catalyst. For both electrochemical reactions, HOR as well as ORR, mostly small platinum particles (≤ 4 nm) dispersed on carbon powder are used as catalyst. Since gases, ions and electrons are involved, the electrochemical reactions can only take place at places accessible to each of these species. As shown in 5, only the three-phase boundaries between membrane ionomer, catalyst and void spaces are suitable reaction sites. However, the reactions are not completely limited to this infinitesimal area, small quantities of reactant gases are able to permeate the membrane material. For high current densities and small voltage losses, thin layers with a high surface area are desired [12].
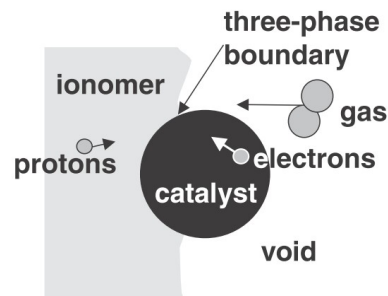
*Figure 5: Reaction sites on the
catalyst surface, depicted from [12]*

Prior to its first practical use, a newly fabricated CCM needs to be conditioned first. The conditioning, also known as activation or break-in, ensures maximized and steady cell performance. For conditioning the cell is usually run under operating conditions for several hours or even days, depending on the conditioning method. During this process, the cell performance increases and finally reaches a plateau. It is not fully understood which changes are taking place in the CCM during the activation, possible explanations are the removal of impurities from the catalyst as well as the hydration of the initially dry membrane [13].

The **gas diffusion layer (GDL)** is located bewteen the CCM and the flow field. It acts as gas diffuser, providing the reactant gases access to the whole CCM area, not just the parts right beneath the flow field channels. It is also important for the removal of product water from the membrane. Furthermore, the GDL mechanically stabilizes the soft membrane and prevents it from sagging into the gas channels. To fulfill those tasks, a porous, rigid, heat and current conducting material is needed. Carbon fiber materials like carbon paper and carbon cloth have shown to be the best option to for those requirements [6].

Fuel cell end plates usually consist of three parts, a **flow field plate**, a metallic **current collector** and a **casing** system to apply the clamping pressure necessary to seal the seal and ensure the fuel cell components contacting each other. Flow field plates feature channels to distribute gases and to remove product water. Most commonly, these channels are serpentine shaped, although various shapes exist, as shown in 6. Recent research shows that some shapes

(like seen in 6 c) may significantly outperform more established ones [14]. **Bipolar plates** house flow fields on both sides and are used in fuel cell stacks, where they connect the separate cells, as shown in 7.
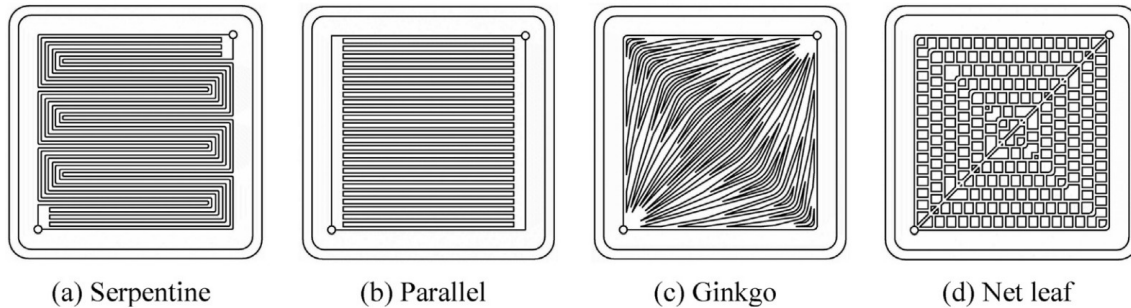

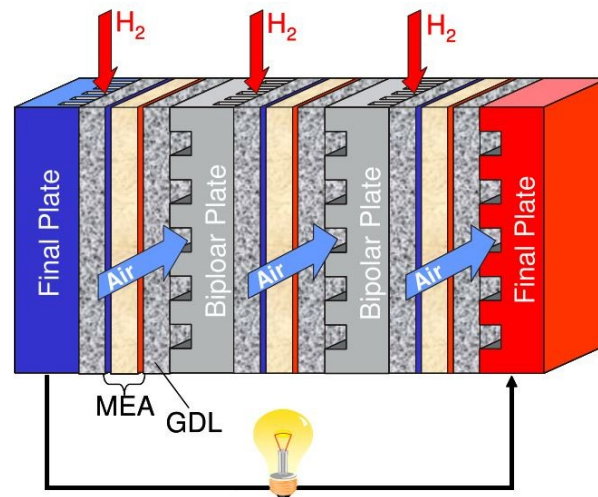*Figure 6: Different flow field shapes applied in PEFCs, depicted from [14]*

Figure 7: Stack assembly of a PEFC, depicted from [15]

Gaskets are essential components of every fuel cell, preventing reactant gases from leaking outside or mixing with each other. Adequate sealing materials need to withstand the exposure of hydrogen, oxygen and humidity as well as mechanical stress. Therefore, silicone based elastomers are commonly used as gaskets in PEFCs [16].

2.3. Fuel cell characterization

To analyze the performance of a fuel cell and to identify sources of losses and degradation, various characterization techniques are required. Since the scope of this work is the testing of different operation conditions on already established cell components, this chapter focuses characterization of the assembled fuel cell rather than the ex situ analysis of single components. In situ electrochemical characterization methods allow gathering information about fuel cell behavior during operating conditions. Moreover, not only the cell components themselves, but also the interfaces between them, which are often a source of losses, can be characterized. Electrochemical experiments focus on three fundamental variables, voltage (V), current (I) and time (t). For better comparison, current density (j) is rather used for fuel cells instead of current. It is calculated by dividing the current by the electrode area of the fuel cell. Since voltage and current (density) are not independent from each other, generally two measuring modes can be distinguished for electrochemical characterization techniques, namely potentiostatic and galvanostatic. Potentiostatic means the voltage is controlled, the resulting current response is measured. Galvanostatic means the opposite way, the current is controlled while the voltage response is measured. For both modes, the controlled variable can be steady-state as well as dynamic. PEFC performance heavily depends on operating conditions, such as cell temperature, reactant gas stoichiometry, pressure and humidity [17].

2.3.1. Polarization curves

A polarization curve, or j-V curve is a plot of cell potential (V) against current density (j), measured at constant operating conditions. Recording polar curves is a straightforward yet powerful method to obtain information about FC performance, i.e. it is simple to distinguish high performing cells from damaged ones. The higher the voltage at any given current density, the better the resulting cell power. As mentioned before, the operating conditions gravely influence the cell performance and thus the shape of the UI curve. Therefore, similar conditions are required for a comparison of different measurements. Usually, polarization curve measurements are done in galvanostatic mode. Therefore an electric load is used to control and consume the current. During

measurement it is very important that the FC is operated in a steady state before recording each data point, otherwise the results are hardly reliable. After each change of current density, the voltage needs time to stabilize again.

Regarding reactant flow rates, there are two options, constant flow rate and constant stoichiometry. In the first case, the value of the gas flow rates is fixed, considering the expected maximum current density of the FC. In the second case, the reactant stoichiometry is set and the flow rates are dynamically adapted to the current density. This is also a factor that has to kept in mind when comparing polarization curves.

As shown in 8, the polarization curve's typical shape is the result of different voltage losses. These losses are depending on the current density, they are also called overpotentials. Due to varying contributions of overpotentials at different current densities, polarization curves can be divided into three major regions.
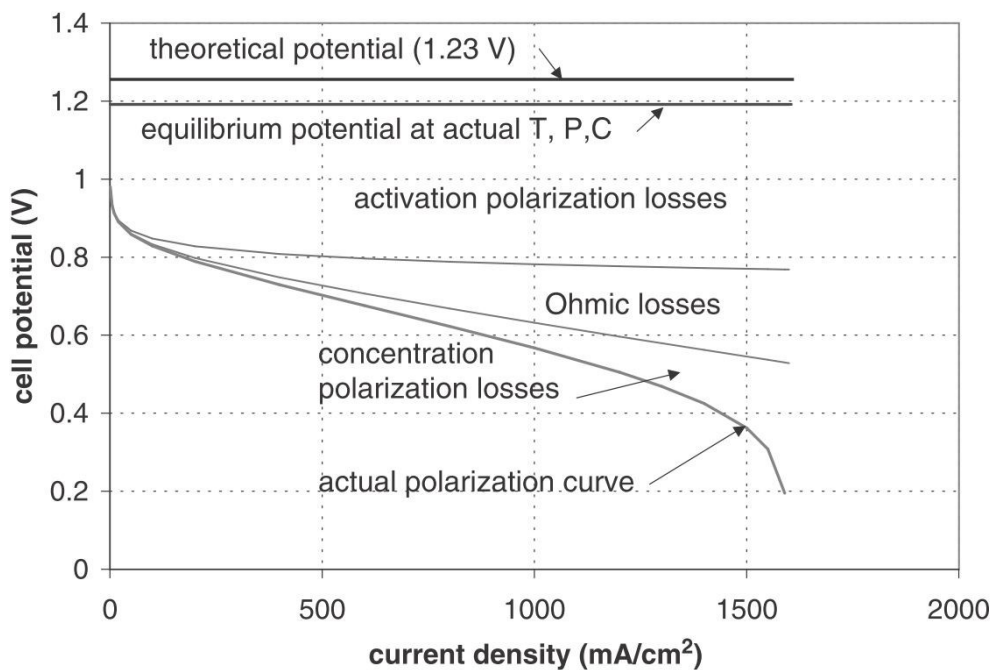

Figure 8: Voltage losses in a fuel cell and the resulting polarization curve, depicted from [9]

At low current densities (0-200 mA cm^{-2}), a sharp voltage drop can be observed. In this region of activation polarization, the slow kinetics of the ORR are responsible for the majority of voltage losses [9]. The correlation between activation overpotential and current density is described by the Butler-Volmer-equation (Equation 12). The exchange current density (j_0) is the is the current

density of the anodic and cathodic partial reactios at equilibrium. The linear part of the curve (200-1200 mA cm^{-2}) is called ohmic region, where voltage drops are mainly caused by the resistances of cell components like electrodes and the electrolyte. The slope of this linear region equals the internal resistance of the system and is described by Ohm's law, as shown in Equation 13.

$$j = j_0 \left[\exp\left(\frac{\alpha * z * F * \eta_a}{R * T} \right) - \exp\left(\frac{(1-\alpha) * z * F * \eta_a}{R\,T} \right) \right] \qquad \text{\textit{Equation 12}}$$

$$\eta_{Ohm} = j * r_i \qquad \text{\textit{Equation 13}}$$

j	current density (A cm^{-2})	R	gas constant (8.31446 J mol^{-1} K^{-1})
j_0	exchange current density (A cm^{-2})	T	temperature (K)
α	symmetry factor (0<α<1)	η_a	activation overpotential (V)
z	number of transferred electrons	η_{Ohm}	ohmic voltage drop (V)
F	Faraday constant (96485 C mol^{-1})	r_i	internal resistance (Ω cm^2)

At high current densities (>1200 mA cm^{-2}), mass transport of the reactants becomes the dominant permormance influencing factor. The amount of reactants able to diffuse through the GLD and CCM is limited, when this limit is reached, i.e. the reactants demanded for the respective currrent density cannot be provided fast enough, the voltage drops rapidly [17]–[19].

From the measured current densities and voltages, the power density of a FC can be calculated with Equation 14, an example for the resulting power curve can be seen in 9.

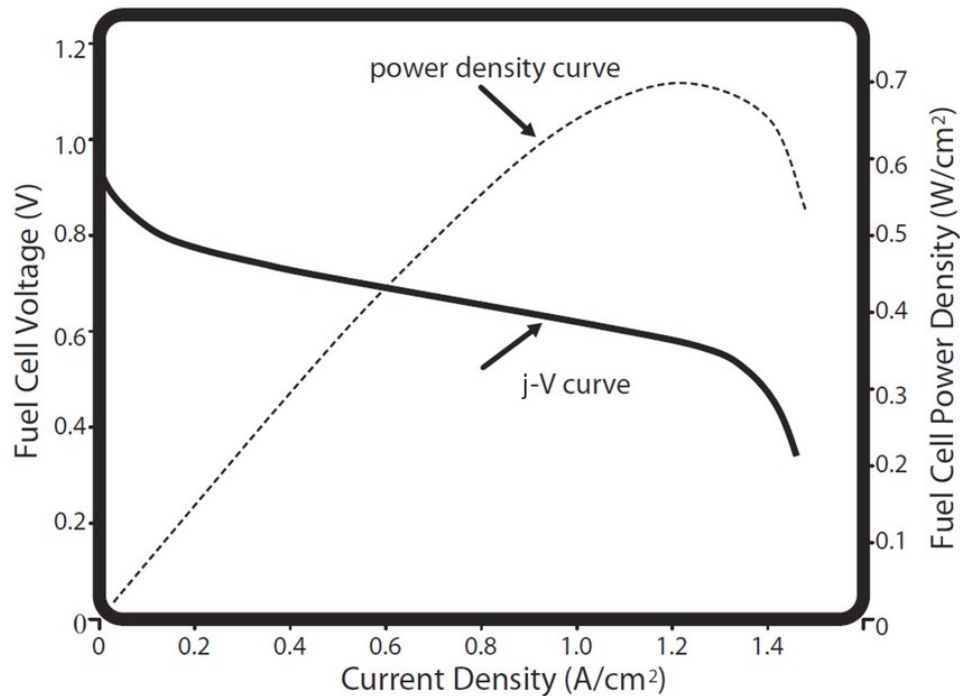$$power\,density = j * V \qquad \text{\textit{Equation 14}}$$

Figure 9: FC polarization curve and corresponding power curve, depicted from [14]

2.3.2. Electrochemical impedance spectroscopy (EIS)

EIS is a non-destructive analysis method suitable for characterization of a wide range of electrochemical systems. Contrary to polarization curves, which visualize the overall FC performance, EIS is capable of resolving individual contributions determining the performance of a FC. Impedance is a measure for a system's effective resistance to an alternating current (AC). Analogous to the resistance against direct current (DC), as descibed by Ohm's law (Equation 15), impedance is a ratio between voltage and current, but in this case both are a function of time (Equation 16). To measure impedance, a sinusoidal voltage or current perturbation is applied to a system, the resulting current or voltage is recorded. The response signal has the same frequency as the applied perturbation, but differs in amplitude and is generally phase shifted (see 10). A sinusoidal impedance can be expressed as presented in Equation 17. Since there is a fundamental relation between trigonometric functions and complex exponential function, the impedance can also be expressed in complex notation, giving Equation 18. Equation 19 shows the relation between frequency of the AC and radial frequency.
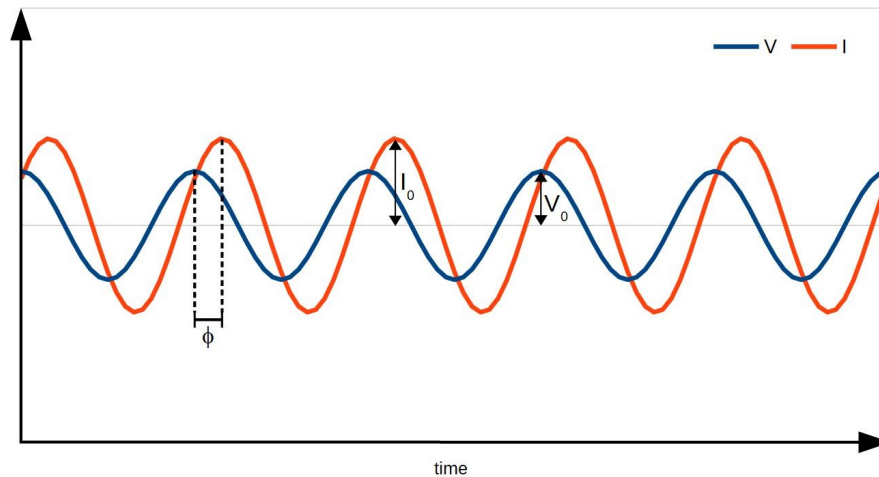
Figure 10: Sinusoidal voltage and phase shifted current response

$$R = \frac{V}{I} \qquad \textit{Equation 15} \qquad\qquad Z = \frac{V(t)}{I(t)} \qquad \textit{Equation 16}$$

$$Z = \frac{V_0 \cos(\omega t)}{I_0 \cos(\omega t - \phi)} = Z_0 \frac{\cos(\omega t)}{\cos(\omega t - \phi)} \qquad \textit{Equation 17}$$

$$Z = \frac{V_0 * e^{(i\omega t)}}{I_0 * e^{(i\omega t - i\phi)}} \qquad \textit{Equation 18} \qquad\qquad \omega = 2\pi * f \qquad \textit{Equation 19}$$

R	resistance (Ω)	V_0	voltage amplitude (V)
Z	impedance (Ω)	I_0	current amplitude (A)
V	voltage (V)	ω	radial frequency (s^{-1})
I	current (A)	f	frequency (Hz)
t	time (s)	i	imaginary number (i=$\sqrt{-1}$)

To record an impedance spectrum, a wide range of frequencies covering several orders of magnitude is applied to the system. FC EIS is generally done under operating conditions, meaning that the alternating signal is applied to the cell in addition to a DC electric load. Therefore, not only an electric load, but also a potentiostat supporting EIS is needed.

The latter one has to be connected parallel to the analyzed cell, otherwise the impedance of the whole setup including the DC load would be measured instead of the impedance of the FC. Irregardless of the mode chosen for the DC load, EIS can be done potentiostatic or galvanostatic. Before impedance

spectra are recorded, the cell has to be operated in a steady-state condition. As mentioned before, the j-V behavior of FCs is nonlinear (see 9), thus impedance spectra measured at difference direct current loads will vastly differ from each other. In order to do a reasonable comparison of EIS data, the current densities as well as the operating conditions need to be similar in each measurement. The perturbation applied to the cell has to be small enough that the investigated portion of the j-V curve can still be assumed to show pseudo-linear behavior.

There are two common variants to illustrate EIS data, the Bode plot and the Nyquist plot. The Bode plot features two graphs, one for the magnitude of the responding signal and one for its phase shift, both plotted versus the frequency. The Nyquist plot expresses impedance with complex numbers, the real part of the impedance is on the x-axis and the negative imaginary part on the y-axis. This variant can be found more often in fuel cell characterization than the Bode-plot. A typical Nyquist plot is shown below in 11.
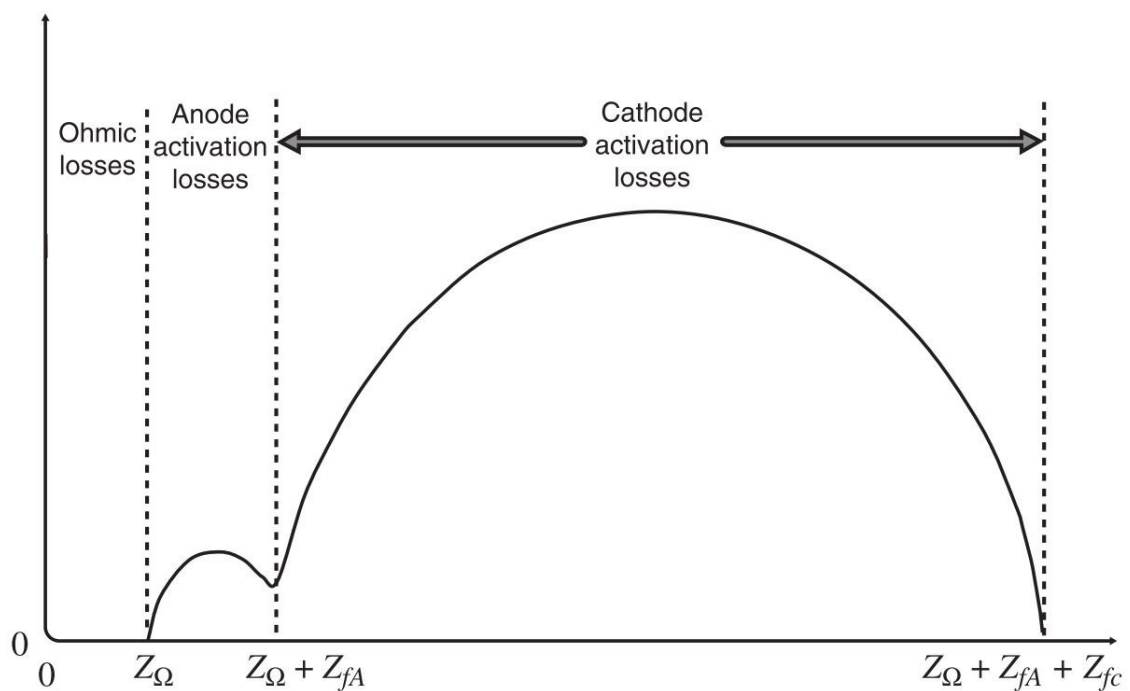

Figure 11: Schematic Nyquist plot of a fuel cell, the different regions of the spectrum can be assigned to different loss mechanisms, depicted from [17]

In a Nyquist plot, the frequency increases from left to right. At high frequencies (>1 kHz, left region of the Nyquist plot), ohmic losses resulting from the properties of the electrolyte mainly contribute to the impedance. The electron transfer between electrodes and electrolyte are reflected by the medium

frequency part (1 kHz-1 Hz, anode and cathode activation losses region in the Nyquist plot). The region at frequencies below 1 Hz is determined by reactant and product transport to and from the electrodes respectively. For exact interpretation of EIS data, equivalent circuit models are needed. Assemblies of circuit elements like resistors, coils or capacitors are used to model a fuel cell's impedance behavior. Although EIS can be a powerful technique for PEFC characterization, spectra interpretation may be very difficult due to the complexity of the porous electrodes and the vast influence of any change in operating conditions. [10], [17], [18], [21]

2.3.3. Cyclic voltammetry (CV)

Cyclic voltammetry is a widespread technique used to characterize fuel cell catalysts and can be done ex situ and in situ. In situ CV is a fast method to determine a fuel cell electrode's electrochemically active surface area (ECSA). In this method, the voltage is swept linearly and with a constant scan rate between an upper and lower limit for multiple times, giving a triangular shaped voltage sequence. The current response is plotted against the voltage, this plot is called cyclic voltammogram. Contrary to polarization curve measurements and EIS, CV characterization of fuel cells is not done with reactants on both electrodes. The voltage signal is applied using a potentiostat, the occurring currents are very low, so an additional electric load is not needed for CV. The working electrode, which is investigated, is purged with an inert gas, such as nitrogen or argon, while hydrogen is fed to the opposing site, acting as counter electrode and reference electrode. For FC characterization, the applied voltage range typically lies between 0.1 mV and 1 V, often lower voltage maxima are used to avoid unnecessary degradation of the FC catalyst support. The scan rates used for CV experiments vary greatly (10^{-4}-10^4 V s^{-1}), although values between 10 mV s^{-1} and 100 mV s^{-1} are most common. Lower scan rates minimize impedance losses and are closer to steady state conditions and are therefore more suitable for ECSA determination. A schematic cyclic voltammogram of a fuel cell is shown in 12.
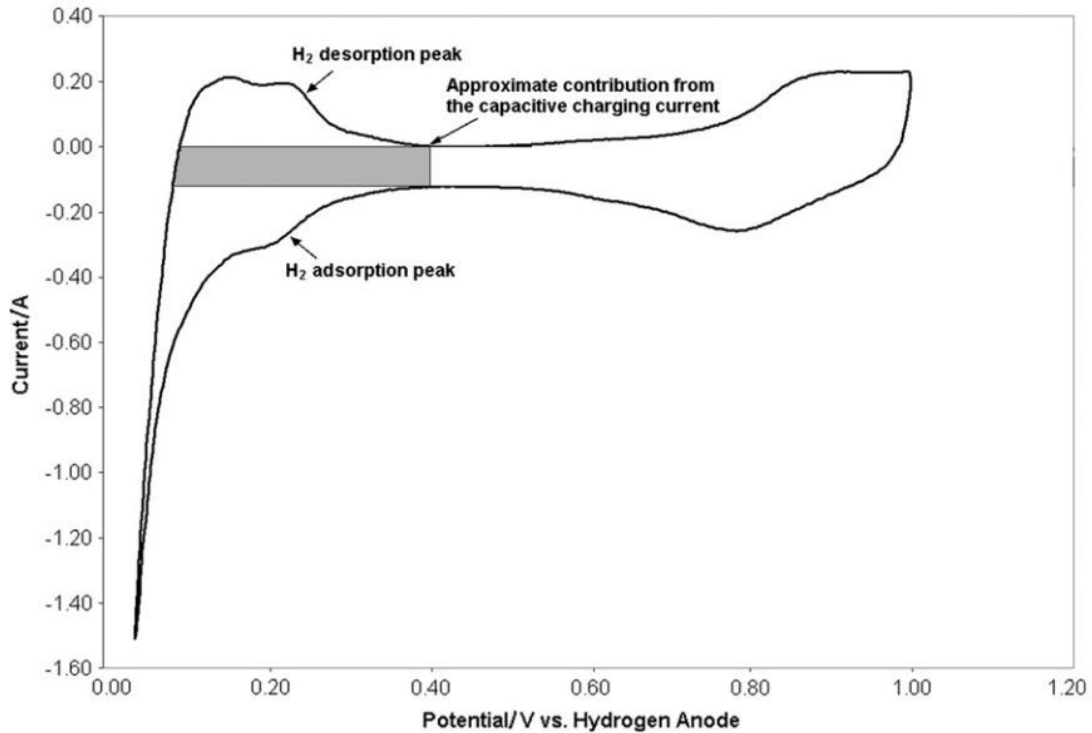
Figure 12: A fuel cell cyclic voltammogram showing peaks of hydrogen adsorption and desorption on a platinum surface, depicted from [21]

While the voltage increases to 0.3 V, H_2 desorption can be observed, at higher voltages (>0.8 V) the Pt surface is oxidized to PtO and PtOH. Decreasing the voltage first leads to Pt reduction (until 0.6 V), followed by H_2 adsorption to Pt at 0.3 V and lower. The current visible between 0.4 V and 0.6 V occurs mainly due to double layer charging and discharging. The areas under the H_2 adsorption and desorption peaks resemble the electrical charge transferred. As a monolayer of H atoms is formed on the Pt surface, the charge can be used to calculate the ECSA of the examined electrode, using Equation 20. [10], [21]

$$ECSA = \frac{Q}{\Gamma * L * A} \qquad\qquad \textit{Equation 20}$$

ECSA	electrochemical active surface area (cm^2 mg^{-1} Pt)
Q	electrical charge (μC)
Γ	H_2 adsorption charge on a smooth Pt surface (210 μC cm^{-2})
L	catalyst Pt loading (mg cm^{-2})
A	electrode Area (cm^2)

2.3.4. Linear sweep voltammetry (LSV)

LSV is a fast method capable of measuring H_2-crossover through the FC membrane, making it useful to determine membrane degradation. The experimental setup and the conditions for LSV are the same as used for CV, with H_2 at the anode and N_2 at the cathode. Unlike CV, a LSV experiment consists only of a single voltage sweep without a backward scan. The sweep starts at 0 V, usually the voltage is not increased further than 0.8 V, this is done to avoid unnecessary Pt oxidation. Since no other reactant species are present at the cathode, the occurring current is only caused by H_2 migrating through the membrane and being oxidized at the cathode. This assumes that there are no or only negligible short currents present in the cell. To quantify electrical short currents, LSV with inert gas at both electrodes can be used. Another difference to CV is that LSV is done with much lower scan rates, mostly below 10 mV s^{-1}. 13 shows a LSV graph measured on a single PEFC. At the beginning of the voltage sweep, the H_2 crossover current rapidly increases with the voltage until it reaches an upper local maximum at approximately 0.3 V. With further increasing voltage the current slightly slightly drops before increasing almost linearly. This is caused by electric short currents present at higher voltages. These short currents usually occur due to membrane thinning, which leads to a decreased electrical resistance of the membrane [22].
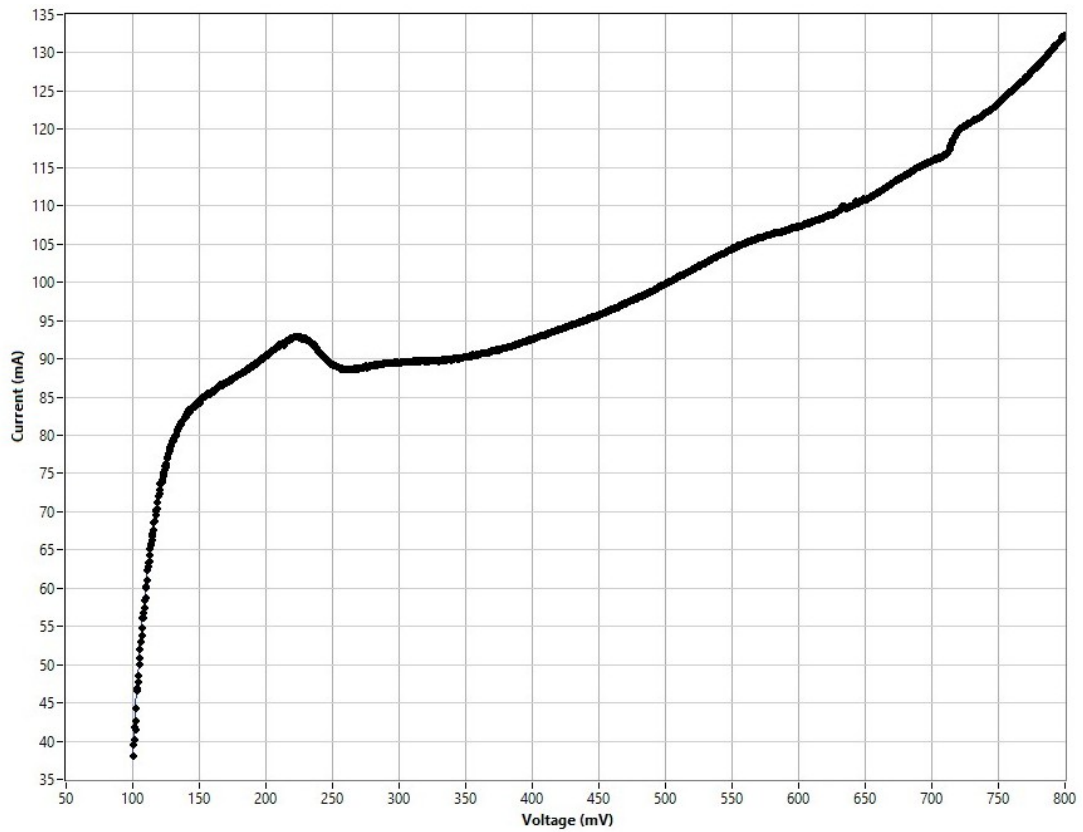
Figure 13: Linear sweep voltammogram of a PEFC, the peak between 200 and 250 mV represents the maximum hydrogen crossover current

To calculate hydrogen crossover, the maximum crossover current is inserted into Faradays law of electrolysis, as shown in Equation 21.

$$r_{hc} = \frac{j_c}{z * F}$$ *Equation 21*

r_{hc}	H$_2$ crossover rate (mol cm^{-2} s^{-2})	z	number of transferred electrons
j_c	crossover current density (A cm^{-2})	F	Faraday constant (96485 C mol^{-1})

2.4. SUSD operation and degradation effects

Running PEFCs under constant load only leads to minor losses, e.g. a stationary PEFC power plant can reach lifetimes of 30000 h [23]. In contrast, dynamic processes as in automotive applications cause significant degradation of cell components, thus a lifespan of even 5000 h is a difficult goal that has not been achieved yet [5]. Pei et al. sorted the various conditions a PEFC faces in automotive application into four categories: load changing, SUSD, high power and idling. Regarding PEFC degradation causes in FCEVs, load changing has the largest impact with 56.50%, followed by SUSD with 33%. The contributions of high power conditions and idling are much less severe, with 5.80% and 4.70% respectively [24].

Considering these data, a significant improvement of cell lifetime can be achieved by optimizing SUSD strategies towards the minimization of harmful conditions. PEFC SUSD sequences consist of multiple steps, during which a variety of degradation mechanisms are possible to happen. Below, an unprotected SUSD process is described [25].

Startup:

1. The cell is shut off, both anode and cathode are filled with air
2. H_2 and air are supplied to the anode and cathode respectively
3. The voltages increases and reaches OCV
4. The cell is ready to operate, current is drawn

Shutdown:

1. The current load is reduced to 0, voltage increases to OCV
2. H_2 and air are shut off, both anode and cathode exhausts are opened
3. Voltage slowly decreases as air enters the anode compartment

During these steps, multiple types of PEFC degradation may take place. In the following paragraphs scenarios leading to accelerated PEFC decay are explained as well as the resulting degradation mechanisms and their consequences,

2.4.1. Formation of H_2/O_2-boundaries

A major amount of PEFC degradation during shutdown can be traced back to the formation of H_2/O_2-boundaries. After shutdown, air enriches in the anode compartment after the H_2 supply is shut off. This can happen either by air entering through the open exhaust, or when air remaining at the cathode migrates to the anode by diffusion through the membrane. As a result, O_2 is present at both electrodes. When the cell is started the next time and the anode is flushed with H_2, a H_2/O_2-boundary is formed and pushed along the flowfield channels. This causes increased potential leading to current reversal and subsequently to accelerated degradation. The exact mechanism of this phenomenon has been first descibed by Reiser et el. in 2005 and can be explained in the following way: When the H_2/O_2-boundary is present in the anode, the cell can be divided into four regions (A-D), as shown in 14. In region A, sufficient amounts of H_2 are present, the potential is nearly 0 V, on the cathode site, the ORR in region B has a potential of approximately 1 V, resulting in the ordinary cell potential of roughly 1 V between A and B. In anode region C, which is still filled whit air, the potential is also close to 1 V. Since region A and C are electrically connected to each other, as well as region B and D are, the potential difference between the anode and cathode is almost uniform. As a consequence, the potential in region D is elevated. [26], [27]

According to Yousfi Steiner et al., in this state the cell can be seen as a fuel cell (A/B) parallel connected to an electrolysis cell (C/D) [28].
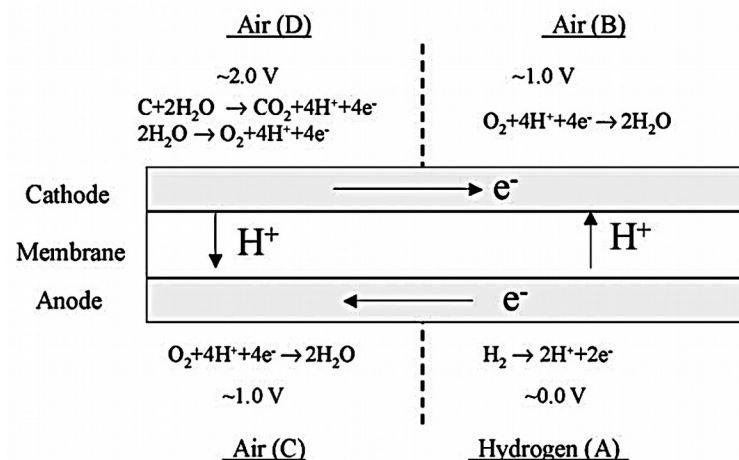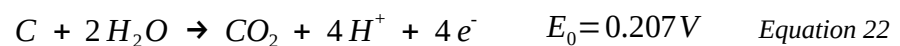

Figure 14: Potentials at different regions along the anode channel
during reverse current conditions, depicted from [27]

In a single cell configuration however, the resulting actual current from A to C

and B to D as well as the corresponding potential differences cannot be measured. Tang et al. has been able to resolve this problem with an experiment featuring two cells. The situation shown in 14 can be simulated by using two PEFCs which have their cathodes connected to each other as well as their anodes. The first cell is operated as usual, with H_2 at the anode (resembling A) and air at the cathode (resembling B), while the second cell is flushed with air on both sites (anode is C, cathode is D). It has been shown that the potential in region D can raise to about 1.75 V, almost twice the OCV. At this potential both water electrolysis and carbon oxidation take place. [27]

The oxidation of carbon materials is a critical issue significantly affecting PEFC durability. Although several cell components like flow field plates and GDLs are usually also made from carbon based materials, corrosion of the catalyst support has the most negative impact on cell performance. The reactions taking place when carbon materials are oxidized are shown in Equation 22 and 23. Despite the low standard potentials, carbon corrosion is usually kinetically hindered during normal PEFC operation. The kinetic barrier of these reactions heavily depends on the operation conditions, higher cell temperatures and cathode gas humidity foster carbon corrosion [29]. Significant CO_2 formation can be observed above 1 V, If the potential is higher than 1.2 V, carbon monoxide (CO) is also formed [30].

$$C + 2H_2O \rightarrow CO_2 + 4H^+ + 4e^- \qquad E_0 = 0.207V \qquad \textit{Equation 22}$$

$$C + H_2O \rightarrow CO + 2H^+ + 2e^- \qquad E_0 = 0.518V \qquad \textit{Equation 23}$$
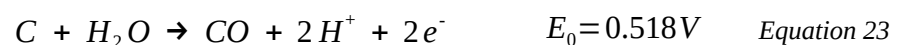
Carbon corrosion of the catalyst support has several negative consequences, such as electrode thinning and decreasing porosity, Pt agglomeration is also fostered, as the attachment of Pt to the support gets weakened. Carbon corrosion may even cause the loss of active catalytic material, when Pt particles completely lose contact to the surrounding material. [27]

2.4.2.   Open circuit voltage (OCV)

OCV occurs during startup as well as during shutdown. At startup, when H2 and air are introduced, OCV builds up but voltage soon increases, as a current is drawn. However at shutdown, when the gas flow is stopped without any active

measures to remove remaining reactants from the cell, it will usually take a long time for the voltage to decrease. While the slow diffusion of air into the anode not only leads to the H_2/O_2-boundary discussed above, it also causes degradation by keeping the cell in OCV over a long time. Long term tests keeping a cell at OCV in a steady state done by Teranishi et al. [31] have shown that these conditions do considerable damage to the interface region between the electrolyte membrane and the cathode catalyst layer. The consequences are severe performance drops, as shown in 15. The decay of the nafion membrane is most likely caused by formation of hydrogen peroxide. Hydrogen peroxide is believed to be a predominant factor responsible for the decomposition of the electrolyte membrane. Peroxide radicals extensively destruct the nafion matrix, resulting in the formation of pinholes and the loss of proton conducting sulfonic acid groups. During fuel cell operation, most H_2O_2 is formed via an incomplete reduction of O_2.. Due to either H_2 crossover or O_2 crossover, H_2O_2 can be produced at the cathode as well as at the anode under OCV conditions. Advanced corrosion of the cathode catalyst can also lead to increased H_2O_2 formation, since the ORR gets hindered. [31]–[34]

Experiments by Chen and Fuller [31] have shown that increased amounts of H_2O_2 can be found at low anode gas humidity and high oxygen partial pressure. Carbon corrosion can also occur due to the relatively high potential.

The damage caused by OCV conditions can be divided in an irreversible and a reversible part. Kundu et al. observed that the potential losses occuring during OCV conditions can be recovered to a large extend (see 16)[35]
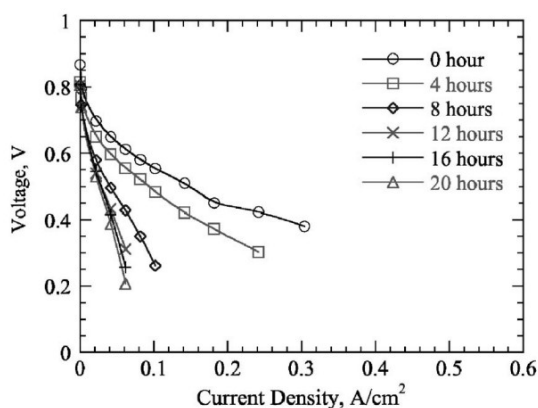
Figure 15: Performance losses caused by idling at OCV, depicted from [31]
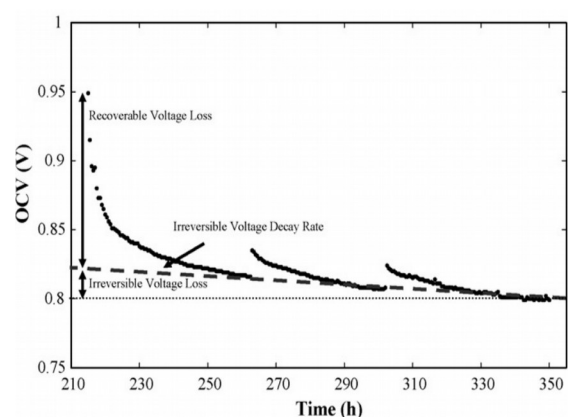
Figure 16: Reversible and irreversible OCV losses, depicted from [35]

The potential recoveries shown were observed after interruptions of the OCV tests, such as polarization curve recordings, maintenance stops and temperature excursions. The characterization included measuring the crossover current and the ECSA, which both changed irreversibly, most likely due to the degradation mechanisms mentioned before. It is assumed that there are different factors contributing to the reversible OCV loss. One reason is the for the most part reversible oxidation/reduction of the Pt catalyst. To a certain degree, pinholes in the membrane may also be temporary sealed by product water condensing at lower temperatures, also recovering some OCV. Membrane swelling by product water increases the resistance for H_2 crossover and may also result in a slightly higher OCV. Similar reasons for voltage recovery have been mentioned by Gazdzicki et al. [36].

2.4.3. Increasing and decreasing load during SUSD

Quick load changes can cause effects similar to those described in the paragraph discussing the formation of H_2/O_2-boundaries. Degradation occurs by local hydrogen starvation if the fuel demand exceeds the available amount, or if the even distribution of hydrogen is hindered, e.g. by water blocking the flowfield channels [37]. It is also assumed that frequently switching the load on and off accelerates catalyst and membrane degradation due to platinum migration and aggregation [38].

2.4.4. Mitigation strategies

A PEFC's durability can be significantly enhanced by choosing the right set of operation parameters during startup and shutdown. Conditions boosting degradation may be avoided or at least the time of their presence could be kept as short as possible. Since using conditions to avoid one degradation cause might foster another one instead, compromises are needed, targeting the reduction of the most harmful sources of fuel cell decay. Regarding the degradation mechanisms previously discussed, the probably most devastating scenario would be leaving a FCEVs cell under OCV conditions after shutdown. Such an unprotected shutdown means the gas supply is simply shut off, usually with the exhausts being open. Depending on the size of the PEFC stack and the geometry of the exhaust lines, exchange of remaining H_2 and air from the

outside may be very slowly, keeping the voltage near OCV for a long time. Even worse, since air enters the cell slowly from one side only, there are H_2-starving regions like shown in 14, causing increased carbon corrosion. To lower the cell voltage to a harmless level for shutdown, at least one reactant has to be removed from the fuel cell. The mildest and most effective way to prevent SUSD degradation would be flushing one or both electrodes with an inert gas, such as nitrogen. While this is a good and common way to handle degradation during fuel cell tests under laboratory conditions, its application in FCEVs would not very beneficial. Besides the disadvantageous cost increase, the whole fuel cell system already demands a lot of space, additional inert gas storage and supply system would significantly lower the systems energy density regarding volume and weight. For everyday mobile FC applications, it is more beneficial to enhance the durability by controlling the H_2 and air supplies and the load drawn from the cell during startup and shutdown. Suitable shutdown conditions can be achieved by either consuming one reactant completely or flushing it out with the gas used at the opposing electrode, giving four different shutdown methods:

- Purging the anode with air
- Purging the cathode with H_2
- Consumption of H_2 at the anode
- Consumption of O_2 at the cathode

Purging an electrode is a straightforward method, it only requires adequate piping to use air or H_2 on both electrodes. Concering the waste of H_2, purging the anode with air is more economical. Both variants solve the OCV problem, cathode H_2 purge will also avoid H_2 starvation. Flushing the anode with air can significantly shorten the time where starvation conditions occur, but is not able to completely avoid them.

While electrode purging can be done irregardless of the used fuel and oxidant, reactant composition plays an important role for the consumption strategies. Consuming the air at the cathode is probably the easiest and most rewarding approach. Air roughly consists of 20% O_2 and 80 % N_2, drawing current after air shutoff finally leaves the cathode in an inert N_2 atmosphere. The anode is constantly exposed to H_2, preventing fuel starvation at startup. If pressure drops occur due to the depletion of O_2, either a small air flow can be maintained

during shutdown, the cathode exhaust left open or the anode pressure can be adjusted to prevent pressure differences. The diffusion of O_2 is relatively slow, so only the cells channels and short sections of the supply and exhaust lines need to be free from O_2, when the voltage is low enough, valves attached closely to the cell's openings are shut to prevent O_2 reentering the cathode. Hydrogen consumption only makes sense if reformate (main components H_2, N_2 and CO_2) is used instead of pure H_2, creating an inert atmosphere at the anode. Although the H_2/O_2 boundary at the anode may also be avoided with this strategy, lowering the H_2 concentration by drawing electric current is essentially forcing fuel starvation, probably nullifying this advantage.

Experiments conducted by Oyarce et al. [25] featured tests of each strategy. All four variants yield formidable improvements to FC durability, compared to an unprotected shutdown. As expected the methods avoiding H_2/O_2 boundaries are significantly superior to those which don't. For the O_2 consumption strategy and the anode air purge strategy, degradation rates of 49 µV per cycle and 183 µV per cycle respectively were determined (at 0.86 A cm^{-2}).

The performance loss caused during SUSD may be additionally mitigated by optimizations concerning the control of the electric load. This might be achieved by decreasing the time the cell is exposed to OCV and alleviate fuel starvation and Pt aggregation by using more gentle load changes.

Therefore, different variants of O_2 consumption SUSD strategies are tested and compared with an anode air purge SUSD strategy. While mainly focused on improving cell durability by avoiding the formation of H_2/O_2 boundaries at the anode, two additional O_2 consumption SUSD strategies are created and invesitaged. Of these, the first aims to avoid damage to the cell caused by OCV conditions, this is achieved by using potentiostatic load control to keep the voltage low. The target of the other modified O_2 consumption SUSD strategy is to mitigate degradation caused by H_2 starvation effects by increasing and decreasing the current load slower, this is done by using multiple stages including waiting times instead of a single ramp.

For comparison a fourth SUSD strategy is tested. To display the effects of H_2/O_2 boundaries during SUSD, purging the anode with air is used as shutdown method.

3. Experimental

3.1. Materials and equipment

3.1.1. Test station and instruments

All experiments described in this chapter were carried out on a G60 PEFC test station manufactured by Greenlight Innovation. The test station can be seen in 17. The piping and instrumentation diagram (P&ID) is shown in 19. The G60 is able to control fuel cell temperature, gas inlet line temperatures, anode and cathode pressure and gas flow rates and gas humidity. The cell is heated and cooled with the test station's liquid coolant loop, distilled water is used as coolant.

The gas supply system allows using H_2 on the anode, air on the cathode and N_2 on both electrodes. Since the original test station lacks the option of supplying air to the anode, the test station is modified for the air purge experiments. The anode air supply line added for this purpose can be seen on the outer left of the P&ID. In order to prevent possible negative effects on other experiments caused by additional dead ends in the gas supply system, these modifications are installed just before the experiments featuring anode air purge and are removed afterwards.

The the electrochemical test equipment consists of the integrated electric load and a Gamry Interface 5000E , which serves as potentiostat/galvanostat and as impedance analyzer.

For the cathode exhaust gas measurements, the test station's cathode exhaust line is connected to an ABB Advance Optima AO2020 continuous gas analyzer.

3.1.2. Software

Emerald Software by Greenlight Innovation is used to control the G60 test station and the Interface 5000E. All of its features, such as setting operation parameters, electrochemical measurements or data logging can either be done manually using the graphical user interface or completely automatically by running scripts. Scripts are created with the Emerald Xcue Editor. EIS and CV data are processed with the Echem Analyst™ Software, exhausts gas data logging is done with Analyze IT Explorer.

3.1.3. Gases

- Hydrogen: ALPHAGAZ™ 1 by Air Liquide, ≥99.999 mol-% purity
- Synthetic air: ALPHAGAZ™ 1 by Air Liquide, 20.5 vol-% O_2, 79.5 vol-% N_2, ≥99.999 mol-% purity
- Nitrogen: ALPHAGAZ™ 1 by Air Liquide, ≥99.999 mol-% purity

3.1.4. PEFC components

Each PEFC used for the SUSD experiments consists of a CCM sandwiched between GDLs, this assembly is clamped into a cell compression unit (CCU). The CCMs with an area of 25 cm^2 are manufactured by Greenerity, they feature a 15 µm Nafion™ membrane from Gore® coated with Pt/C catalyst made by Umicore. The Pt loading is 0.05 mg cm^{-2} on the anode and 0.25 mg cm^{-2} on the cathode. PTFE-treated carbon fiber paper of the type H14C7 manufactured by Freudenberg Performance Materials is used as GDL. It is 175 µm thick (145 µm@1 MPa pressure), its area weight is 100 g m^{-2} and it has a microporous layer on one side [39]. The CCU of the type qCf FC25/100 Liquid Cooling manufactured by balticFuelCells consists of two major components, the cell fixture (18) and the support frame (17). The cell fixture includes graphite flowfield plates with a meander of five parallel channels. The support frame features a pneumatic cylinder able to apply a broad range of clamping pressure, depending on the air pressure it is supplied with. Coolant loops in the CCU allow external heating and cooling of the cell which is done with the test stations coolant loop.
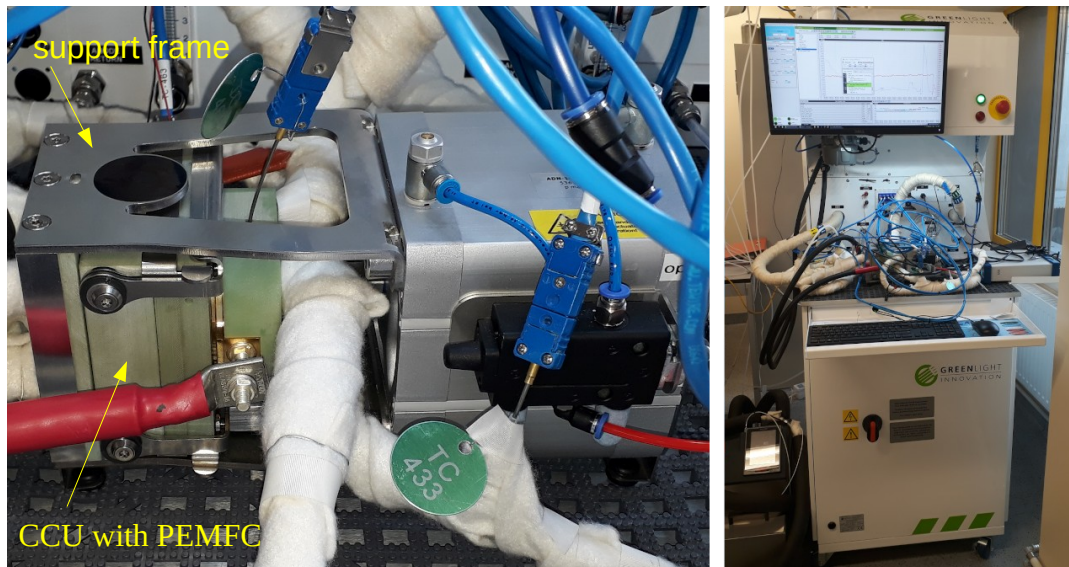
Figure 17: Left: assembled cell, clamped into the compression unit and connected to the test station, right: Greenlight Innovations G60 test station
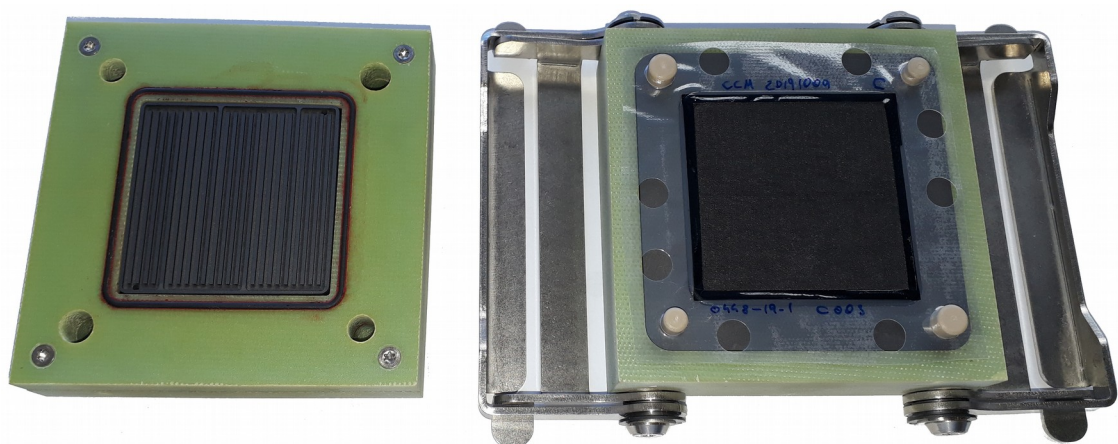
Figure 18: Disassembled cell with fixture unit, CCM and GDL on the right part
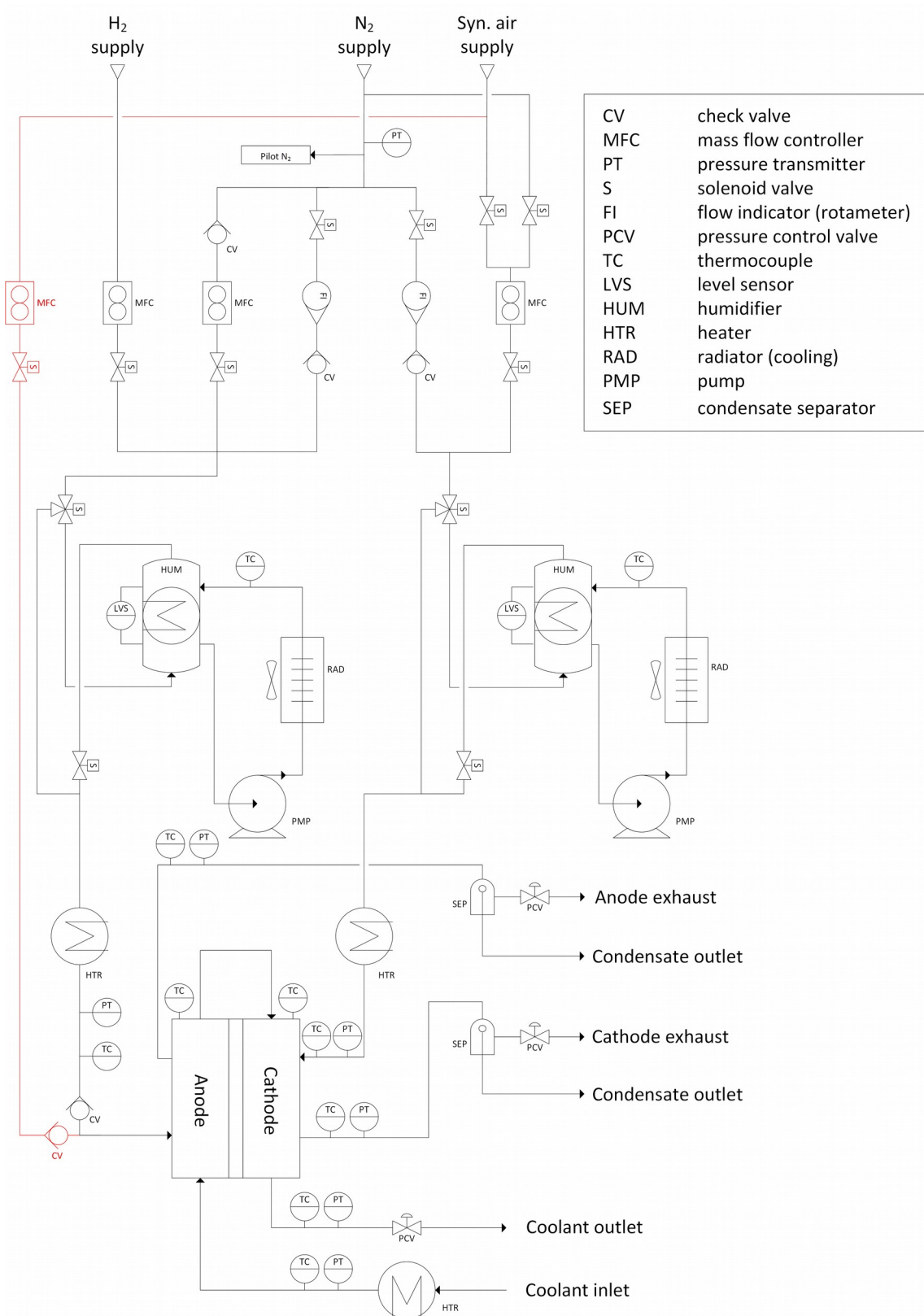
Figure 19: P&ID of the modified G60 PEFC test station, the anode air supply line (colored red) which was added for the anode air purge SUSD strategy.

3.2. Experimental procedure
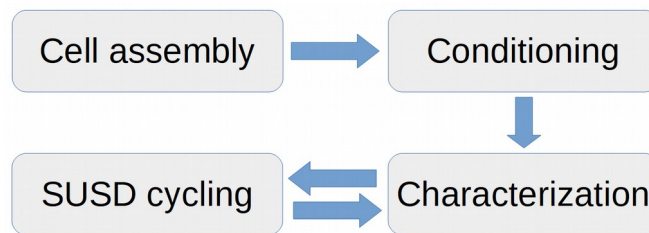
Figure 20: Major steps of the experimental procedure

An overview of the major experimental steps carried out while testing each SUSD strategy is given in 20. After assembling, the cell was conditioned and characterized before performing SUSD cycling. The operating conditions, such as temperature (T), relative humidity (RH) and pressure (p) for the conditioning, characterization and the SUSD experiments are summarized in 1. The individual steps are described in detail in the following sections.

Table 1: Overview of operating conditions during the experiments

parameter	unit	conditioning	SUSD	jV & EIS	CV & LSV
T_{cell}	°C	80	80	80	80
T_{inlet}	°C	85	85	85	85
$T_{dewpoint, anode}$	°C	75	75	75	75
$T_{dewpoint, cathode}$	°C	75	53	53	75
RH_{anode}	-	80%	80%	80%	80%
$RH_{cathode}$	-	80%	30%	30%	80%
p_{system}	kPag	100	0	100	0

3.3. FC assembly

For each SUSD strategy, a new CCM and new GDLs are used. The membrane is cut in shape and holes are punched to fit in the CCU, for the GDLs 5 cm x 5 cm squares are cut out of the carbon paper. The components are placed in the fixture unit, as shown in 18, with the coarse side of the GDL on the outside. The fixture unit is closed, put into the support frame and sealed with the pneumatic piston. Compressed air is applied with a pressure of 5 bar, according to the CCU manual, this corresponds to a clamping pressure of approximately 1.5 N mm^{-2}. Finally the cell is connected with the test station's gas and coolant lines and the electric load.

3.4. CCM conditioning

Prior to any SUSD experiments, the new CCM needs to be conditioned first. This ensures maximized and steady cell performance and a comparable starting situation for each SUSD strategy. Conditioning is done by potential cycling similar to the method described by Bezmalinović et al. [40]. Prior to conditioning, the cell, the humidifiers and the gas inlet pipes are heated, during the warmup phase, N_2 is applied to both anode and cathode with a flow rate of 0.2 NLPM at ambient pressure. To avoid flooding the cell, a script is used to ensure the temperatures inside the humidifiers are always below those of the corresponding electrode. After the target temperatures are reached, N_2 is shut off, reactant gases are applied at 0.5 NLPM and the pressure is increased to 1 bar on both sides. The flow rates are then changed to 0.42 NLPM H_2 at the anode and 1.26 NLPM air at the cathode. The load is turned on (potentiostatic mode) and the potential is varied between 0.4 V, 0.5V and 0.6 V during four hours. Each set potential is kept for 60 s, ramping up and down takes 30 s each (see 21). The exact conditions are shown in 1. The state of conditioned cell prior to any SUSD cycling tests is referred to as BOL (begin of life).
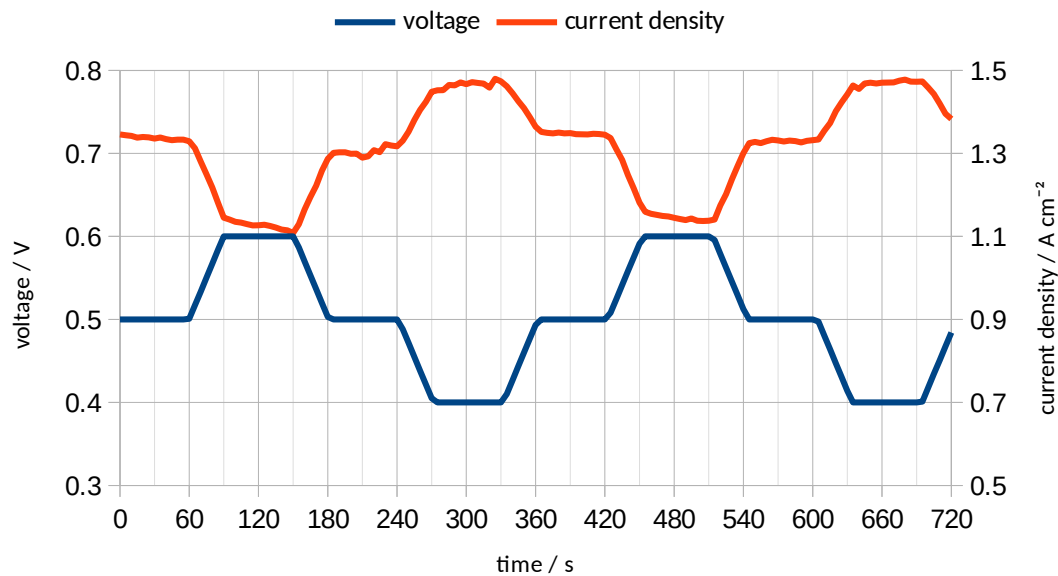
Figure 21: Voltage and current density during V-cycling conditioning (2 cycles)

3.5. FC characterization

Electrochemical characterization is done for every test cell before the beginning of the first SUSD cycling experiment (BOL) and after each 150 SUSD cycles. The electrochemical characterization sequence consists of CV, LSV, polarization curve measurement and EIS done in this order. Exhaust gas measurements are done once for every SUSD strategy after the regular cycling experiments are finished.

3.5.1. Cyclic voltammetry (CV)

For CV, the cell is connected with the Gamry Interface 5000E, the cathode acts as working electrode, the anode is both reference and counter electrode. The anode flow is set to 0.2 NLPM H_2, the cathode flow to 0.2 NLPM N_2. The measurement is done at ambient pressure, with a cell temperature of 80 °C and 80% RH on both electrodes. The voltage is cycled between 0.1 V and 0.8 V with a scan rate of 100 mV s^{-1} For each CV measurement, four cycles are recorded, the triangular voltage pattern is shown in 22.
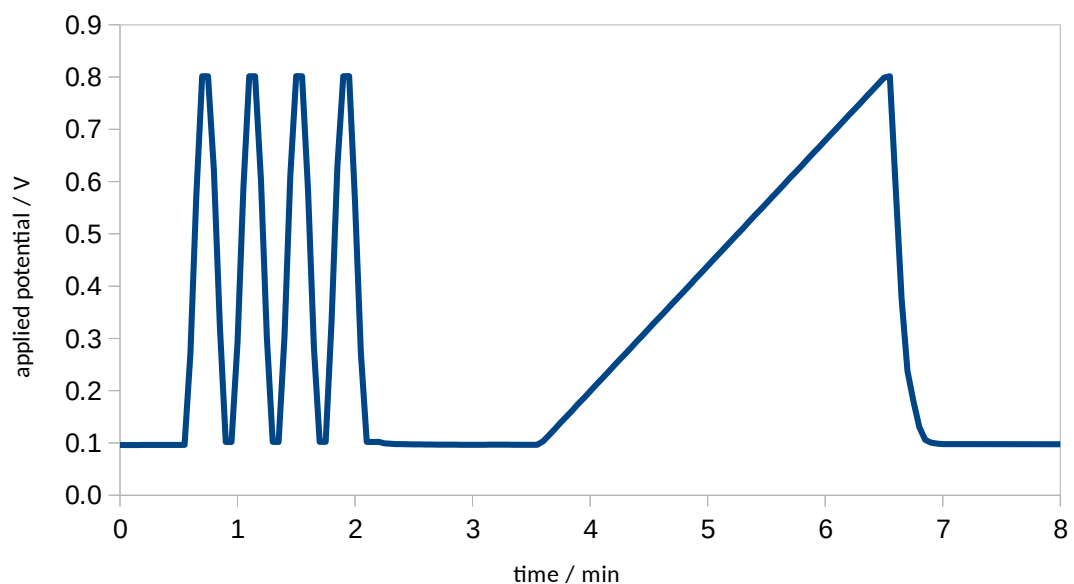
Figure 22: Triangular voltage applied during CV (left, 4 cycles) and LSV (right)

3.5.2. Linear sweep voltammetry (LSV)

LSV is done with the same setup and conditions as CV, the Interface 5000E is set to LSV mode, then a single voltage sweep from 0.1 V to 0.8 V is applied (see 22), the scan rate is 4 mV s^{-1}.

3.5.3. Polarization curve measurement

The polarization curves are recorded at 80 °C cell temperature and 1 bar gauge pressure. The reactant gas flows are set to constant stoichiometry mode, this means the gas flow rates are adapted to the actual current. The stoichiometry factors are 1.4 for H_2 and 2.3 for the synthetic air. The current density (j) is controlled by a script, it increases until either 2 A cm^{-2} are reached or the voltage (V) drops to 0.26 V or lower. The curve is recorded while the current density is decreased again. During the beginning and the end of the recording small current steps are taken, larger steps are used in the linear part of the curve. The j and V data are recorded as soon as V stabilizes at each point. A plot of the applied current density is presented in 23.
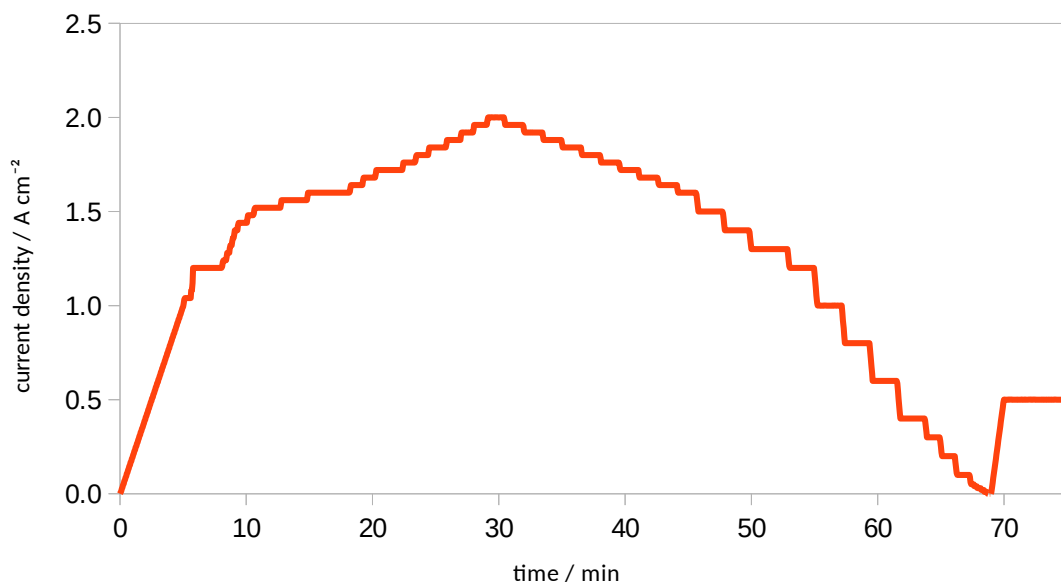
Figure 23: Example of the current density sequence during a polarization curve recording

3.5.4. Electrochemical impedance spectroscopy (EIS)

EIS is carried out with the operating conditions (1) and settings for the gas flows which were used during the polarization curve measurement. When the polarization curve is finished, the current density is ramped up to 0.5 A cm^{-2}. After the cell has stabilized, a 1.25 A AC perturbation is applied. The frequency range is 10 kHz-1 Hz, 10 points per decade are recorded. The equivalent circuit used to fit the EIS data is shown in 24.
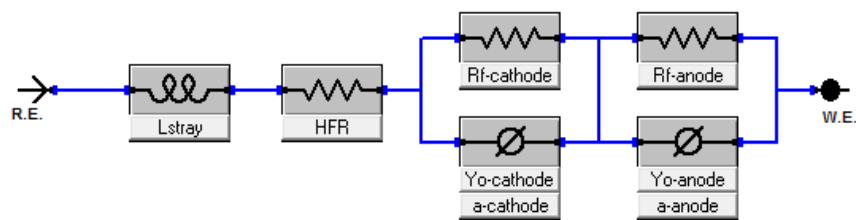
Figure 24: Equivalent circuit model used for EIS data interpretation

3.5.5. Exhaust gas measurement

In the cathode exhaust gas, CO, CO_2 and O_2 contents are measured after the 450 SUSD cycles. The cathode exhaust line is connected to the gas analyzer and 20 SUSD cycles are carried out. The operating conditions are similar to the SUSD experiments, except the pressure is increased from ambient pressure to 50 kPag. This is necessary due to the resistance of the gas analyzer.

3.6. SUSD cycling

The SUSD experiments includes testing four different strategies. Of these strategies, the first three are done with oxygen consumption shutdown, varying in the way the electric load is applied. In the first SUSD strategy, after the reactant gas supply is turned on it is waited until the voltage raises to OCV and is then kept in this state for a short time before the load is applied. The voltage also reaches OCV during the shutdown sequence, the O_2 consumption is started afterwards. The second strategy aims to avoid voltages beyond 0.8 V, to reach this, potentiostatic load control is used during the startup and shutdown sequences. The third strategy is similar to the first one, except the current is raised and decreased in multiple steps. For comparison, a fourth strategy where the anode is purged with air during shutdown is tested, its load pattern is similar to the first strategy.

The SUSD cycling experiments are carried out with the temperature, pressure and relative gas humidity stated in 1. Of each SUSD strategy 450 cycles are applied, prior to the first cycle and after every 150 cycles, the procedure is stopped and the cell is electrochemically characterized. The cycling is done automatically. The voltage and current density sequences are shown in 25-28.

3.6.1. SUSD strategy 1
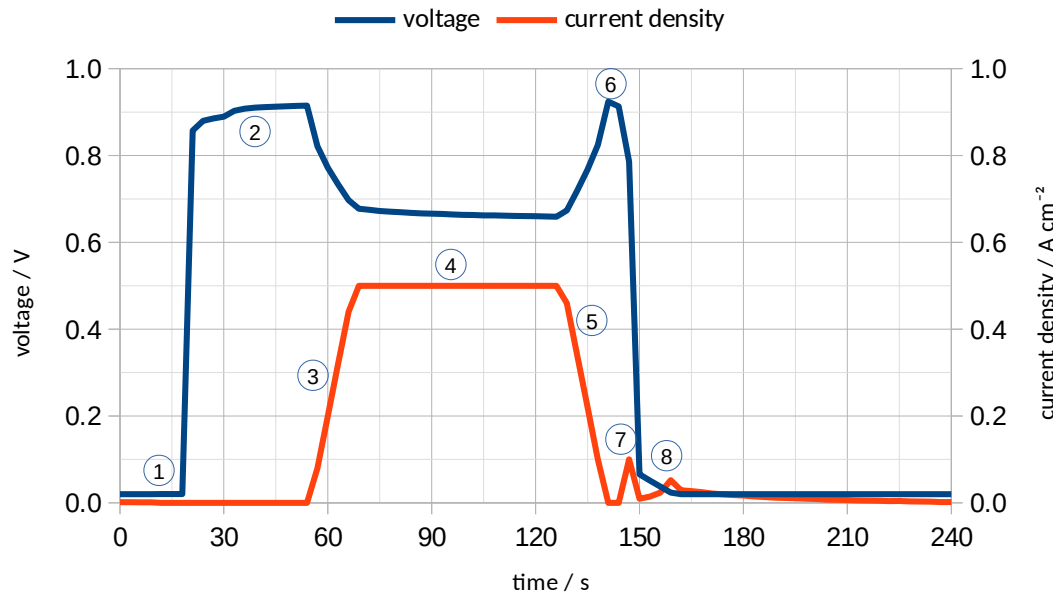
Figure 25: V and j sequence for one cycle of SUSD 1

This is the O_2 consumption strategy which is used as reference strategy. After a short period of OCV, a galvanostatic load is applied for one minute. The shutdown sequence consists of a short current pulse, afterwards the load is changed to potentiostatic mode, this is done to prevent negative voltages, which occurred during pretests. To avoid reactant gas diffusion from the humidifier into the cell during shutdown, the dry bypass is opened (and the humidifier closed) when the gas supply is shut off. SUSD strategy 1 includes the following steps:

1. reactant gases are turned on (0.2 NLPM H2, 0.8 NLPM syn. air), V increases
2. V is kept >0.9 V for 20 s
3. current load is increased from 0 to 0.5 A cm^{-2} during 12.5 s (rate=1 A s^{-1})
4. current load is kept constant at 0.5 A cm^{-2} for 60 s
5. current load is decreased from 0.5 A cm^{-2} to 0 during 12.5 s (rate=1 A s^{-1})
6. cathode air is shut off, wait 5 s
7. a current load of 0.1 mA cm^{-2} is applied until V drops below 0.2 V
8. V is potentiostatically kept at 20 mV until j drops stays below 2 mA cm^{-2}, load is then turned off

3.6.2.   SUSD strategy 2
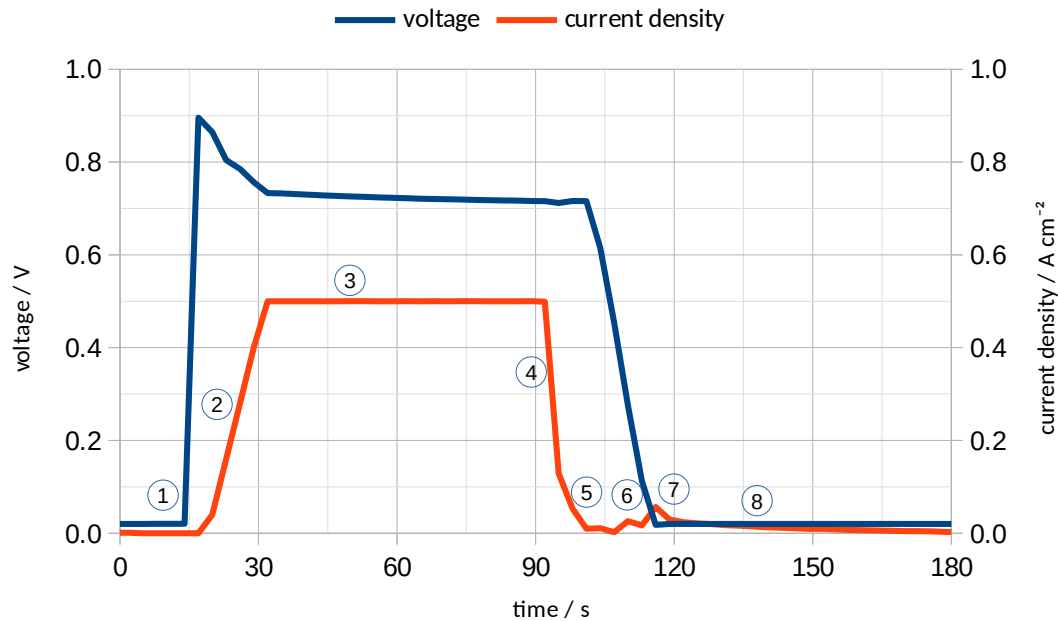
Figure 26: V and j sequence for one cycle of SUSD 2

In this strategy, voltages close to OCV are avoided by increasing the current load shortly after the reactant gases re turned on. During shutdown, the voltage is ramped down potentiostatically. Step 2, 7 and 8 differ from SUSD strategy 1, the other steps are the same. SUSD strategy 2 includes the following steps:

1. reactant gases are turned on (0.2 NLPM H2, 0.8 NLPM syn. air),wait one second, V increases
2. current load is increased from 0 to 0.5 A cm^{-2} during 12.5 s (rate=1 A s^{-1})
3. current load is kept constant at 0.5 A cm^{-2} for 60 s
4. current load is decreased from 0.5 A cm^{-2} to 0 during 12.5 s (rate=1 A s^{-1})
5. cathode air is shut off
6. load is changed to potentiostatic mode
7. after j<8 mA cm^{-2}, V is ramped down to 20 mV during 12.5 s
8. V is potentiostatically kept at 20 mV until j drops stays below 2 mA cm^{-2}, load is then turned off

3.6.3.   SUSD strategy 3
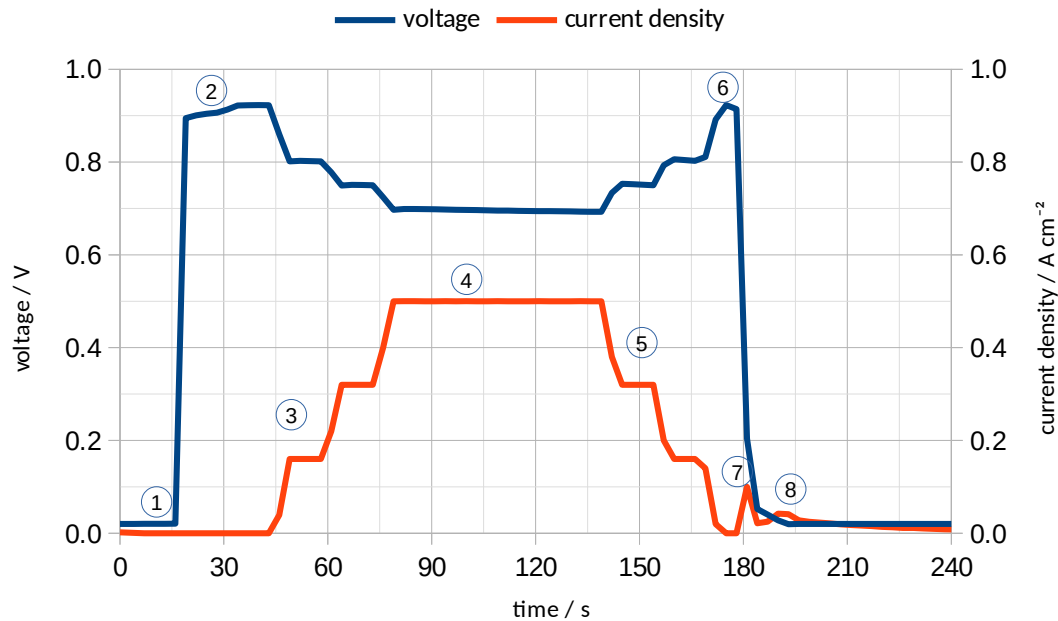
Figure 27: V and j sequence for one cycle of SUSD 3

The third strategy is similar to the first, except the current load is increased and decreased in stages. SUSD strategy 3 includes the following steps:

1. reactant gases are turned on (0.2 NLPM H2, 0.8 NLPM syn. air), V increases
2. V is kept >0.9 V for 20 s
3. current load is increased in stages from 0 to 0.5 A cm^{-2} (rate=1 A s^{-1}), j is kept constant for 10 s at 0.16 and 0.32 A cm^{-2}
4. current load is kept constant at 0.5 A cm^{-2} for 60 s
5. current load is decreased from 0.5 A cm^{-2} to 0 during 12.5 s (rate=1 A s^{-1})
6. cathode air is shut off, wait time of 5 s
7. a current load of 0.1 A cm^{-2} A cm^{-2} is applied until V drops below 0.2 V
8. V is potentiostatically kept at 20 mV until j drops stays below 2 mA cm^{-2}, load is then turned off

3.6.4. SUSD strategy 4
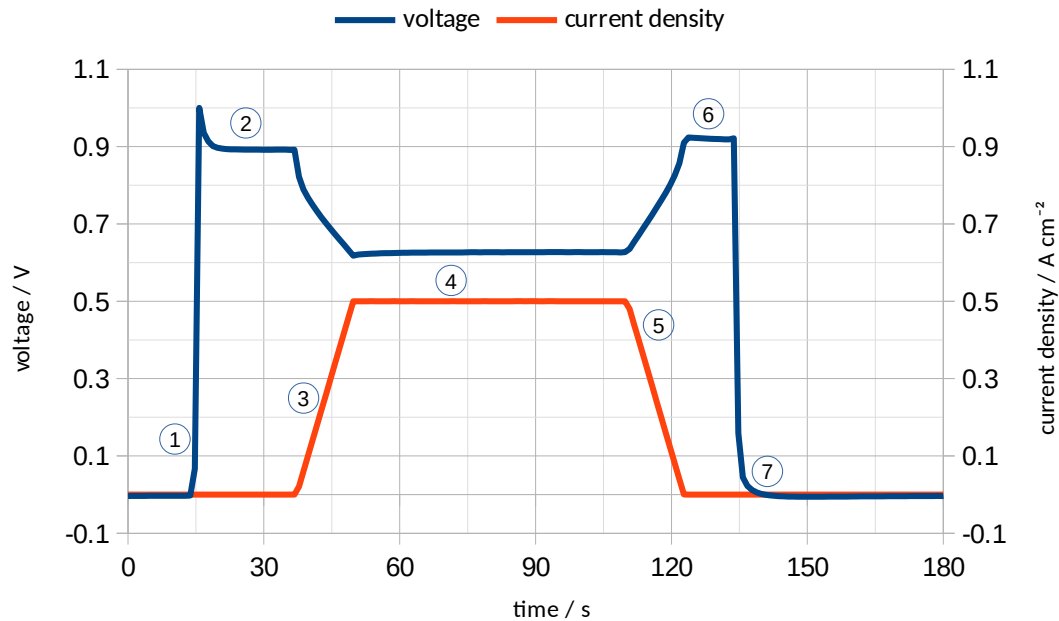
Figure 28: V and j sequence for one cycle of SUSD 4

SUSD strategy 4 includes the simulation of a H_2/O_2 boundary at the anode. This strategy has a similar startup procedure as SUSD #1, the voltage limit in step 2 is lowered from 0.9 V to 0.7 V, as the OCV is expected to significantly decrease during cycling. Unlike the previous strategies, the electric load is not used after the current is decreased to zero, the shutdown solely consists of purging the anode with air, quickly removing H_2 and causing the voltage to drop close to zero.

1. reactant gases are turned on (0.2 NLPM H2, 0.8 NLPM syn. air), V increases
2. V is kept >0.7 V for 20 s
3. current load is increased from 0 to 0.5 A cm^{-2} during 12.5 s (rate=1 A s^{-1})
4. current load is kept constant at 0.5 A cm^{-2} for 60 s
5. current load is decreased from 0.5 A cm^{-2} to 0 during 12.5 s (rate=1 A s^{-1})
6. load is turned off, wait time of 10 s, V increases to OCV
7. H_2 is shut off, anode is purged with 0.5 NLPM air for 60 s

4.　Results and discussion

4.1. Voltage decrease while applying SUSD strategies 1-4

The voltage response while the 0.5 A cm^{-2} load is applied during all SUSD strategies is shown in 29. The values presented are mean voltages of the last 20 recorded data points during the current load application. It can be observed that each strategy shows different behavior in the way the voltage decreases during SUSD cycling. The voltage graphs of SUSD 1 and SUSD 2 look quite similar, with SUSD 1 being a bit more irregular, as it has more plateaus as well as steeper sections. Both strategies show a lower voltage at the first cycle of each series (cycle 1, 151 and 301). After those cycles the voltage stabilizes to values comparable to the end section of the previous cycling series. The opposite can be observed for SUSD 3 and SUSD 4, as for both strategies regeneration seems to take place while the cell is shut of cooled to room temperature after each series of 150 cycles. For SUSD 3, an explanation might be the fact that due to the stepped and thus slower rates for current increase and decrease, the cell is kept at higher voltages for a longer time. As mentioned before, e.g. oxidation of the Pt catalyst caused by OCV might show high reversibility, as reduction takes place when the voltage is again lowered. The same is possible for SUSD 4, where high internal potential differences occur when H_2/O_2 boundaries are present at the anode. Besides this, SUSD 3 shows the smallest voltage decay while under load compared to the other strategies. SUSD 4 shows the most voltage drop, indicating that H_2/O_2 boundaries induce performance limiting degradation effects. A striking difference between SUSD 4 and the other strategies is its already low voltage prior to any cycling, which is roughly at the same level as the other strategies' terminal voltages after 450 cycles. This suggests, that there might be some air at the anode during the whole experiment, which cannot be completely removed from dead ends in the system while H_2 is supplied to the anode, resulting in mixed potentials, hence lower voltage and possibly more degradation.
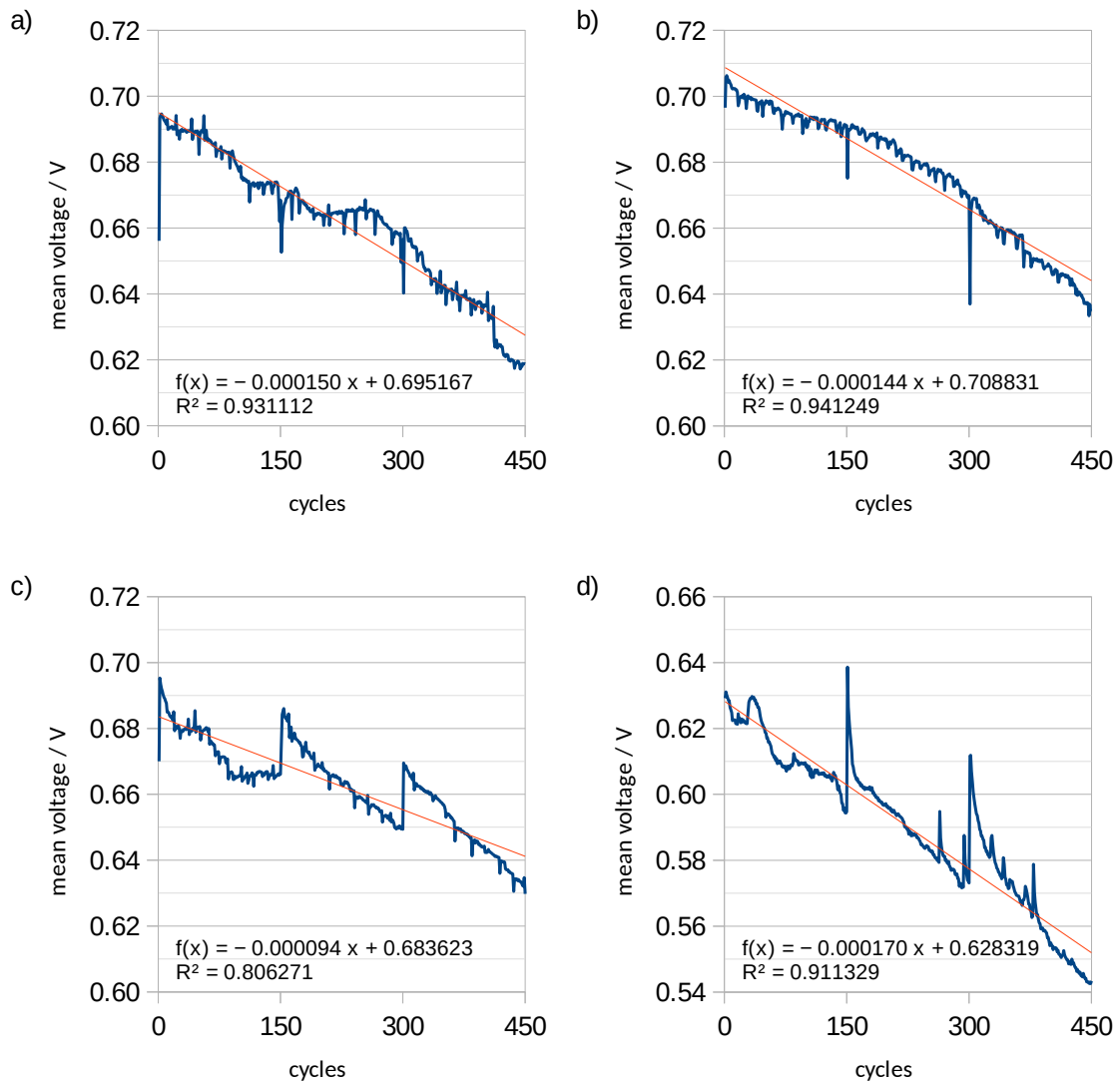
Figure 29: Mean voltage at 0.5 A cm^{-2} during cycling experiments of a) SUSD strategy 1, b) SUSD strategy 2, c) SUSD strategy 3 and d) SUSD strategy 4

4.2. Polarization and power curves of SUSD strategies 1-4

SUSD strategies 1-3 show a similar pattern concerning polarization curves, as can be seen in 30. In a current density range from 0-1.2 A cm^{-2}, the voltage significantly drops after the whole 450 cycle procedure. Whereby the differences after each series of 150 cycles are not significant though. At high current densities, SUSD 1-3 seem to have no negative impact on performance, there is even a minor improvement in the diffusion controlled areas of the curve after cycling, although this does not seem to properly correlate with the number of cycles. The reason for this behavior might be that the chosen conditioning time of only four hours is insufficient. Another one could be that with ongoing carbon corrosion at the cathode may partially increase the surface area, so O$_2$

diffusion is possibly improved to some extend. At high currents, a lot of heat is produced in the cell, causing changes in gas humidity which cannot be quickly corrected by the relatively sluggish coolant system. In contrast to the first three strategies, SUSD 4 results in increased voltages at all regions of the polarization curve as well a clearly visible correlation of performance decay with the number of cycles. The overall negative impact SUSD strategy 4 due to the occurring H_2/O_2 boundaries is also much more severe than those of the other strategies.
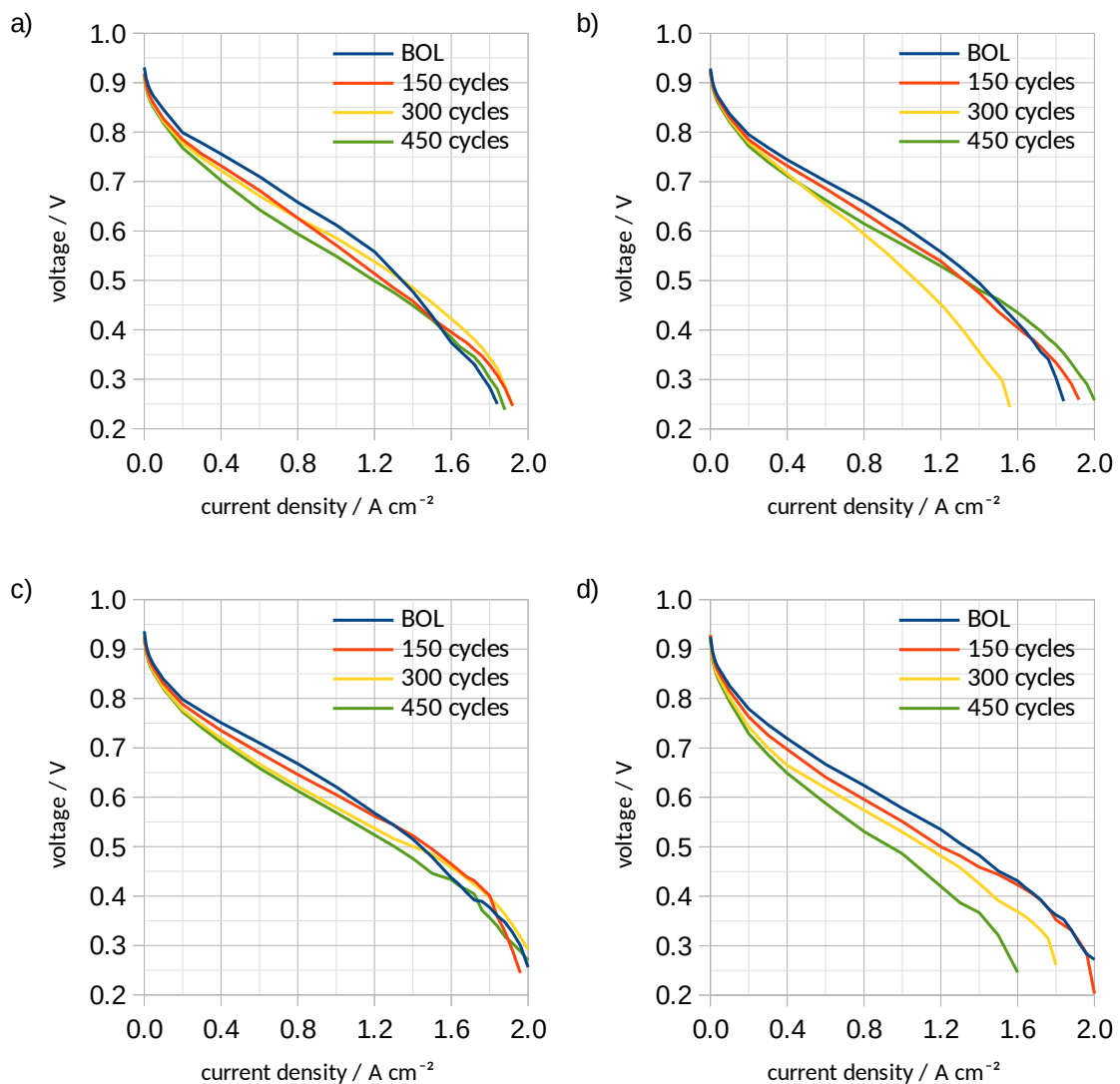
Figure 30: Polarization curves recorded at BOL and after each 150 cycles of a) SUSD strategy 1, b) SUSD strategy 2, c) SUSD strategy 3, and d) SUSD strategy 4

The polarization curve recorded after 300 cycles of SUSD strategy 2 shows a remarkable effect. What looks like an outlier at first glance, is a reproducible

result. Usually SUSD cycling was done overnight, after the last cycle was finished, the test station was shut off and the cell was allowed to cool down to room temperature for several hours until characterization was done. In this particular case, the cell was characterized right after cycling, with no rest time or cooldown in between. As a result, a large performance drop can be seen in the respective polarization curve (30 b). After the next 150 cycles, cooling down and waiting, the cell shows no such performance decay. Its voltage in the ohmic (linear) region of the curve is only slightly below the one recorded at BOL, in the diffusion controlled region, it even performs better. Since the detailed investigation of regenerative effects is not in the scope of this thesis, cooldown and a resting time of at least three hours before cell characterization was ensured for subsequent cycling experiments.

OCV tends to decrease with ongoing cycling (see 2), although those voltage drops are very small for all four strategies, with SUSD strategies 2 and 4 having slightly less impact. This is no surprise for the second strategy, as its aim is to avoid high voltage situations known for cause OCV drops. This is not the case for SUSD 4, which has almost exactly the same current profile as SUSD 1, with additional high voltage peaks due to the H_2/O_2-fronts.

Table 2: OCV measured during polarization curve recording and total OCV loss for SUSD strategies 1-4

cycles	OCV / V			
	SUSD 1	**SUSD 2**	**SUSD 3**	**SUSD 4**
0	0.931	0.929	0.936	0.925
150	0.919	0.925	0.926	0.929
300	0.915	0.920	0.922	0.924
450	0.912	0.920	0.918	0.917
Δ0-450	**-0.019**	**-0.009**	**-0.018**	**-0.008**

31 shows the corrected polarization curves, where the voltage losses caused by ohmic resistance are excluded to give a better visibility of activation losses. The calculated specific ohmic resistances are presented in 3. The activation losses tend to grow with an increasing number of cycles, although barely any differences can be seen from 300 to 450 cycles with SUSD 3 and 4. While the losses are in the same order of magnitude for all strategies, the cell used for

SUSD 4 already shows higher activation losses at BOL. As well as the lower mean voltage in 29 d, this may be a hint for air leaking into the anode channels even though the valve is closed. Concerning the specific ohmic resistance, there is no discernible trend within the calculated values. If comparing only the values before the first and after the last cycles, only SUSD 4 shows a clear difference, with the specific resistance increasing by 51 mΩ cm^2. Interestingly, the curve of SUSD 2 after 300 cycles (31 b) shows slightly lower activation losses than the curve at BOL. With the current density increasing from 0 to 0.4 A cm^{-2} the activation loss is -93 mV at BOL and -79 mV after 300 cycles. However, after 300 cycles of SUSD 2 the cell exhibits by far the highest specific ohmic resistance of all measurements done (see 3).
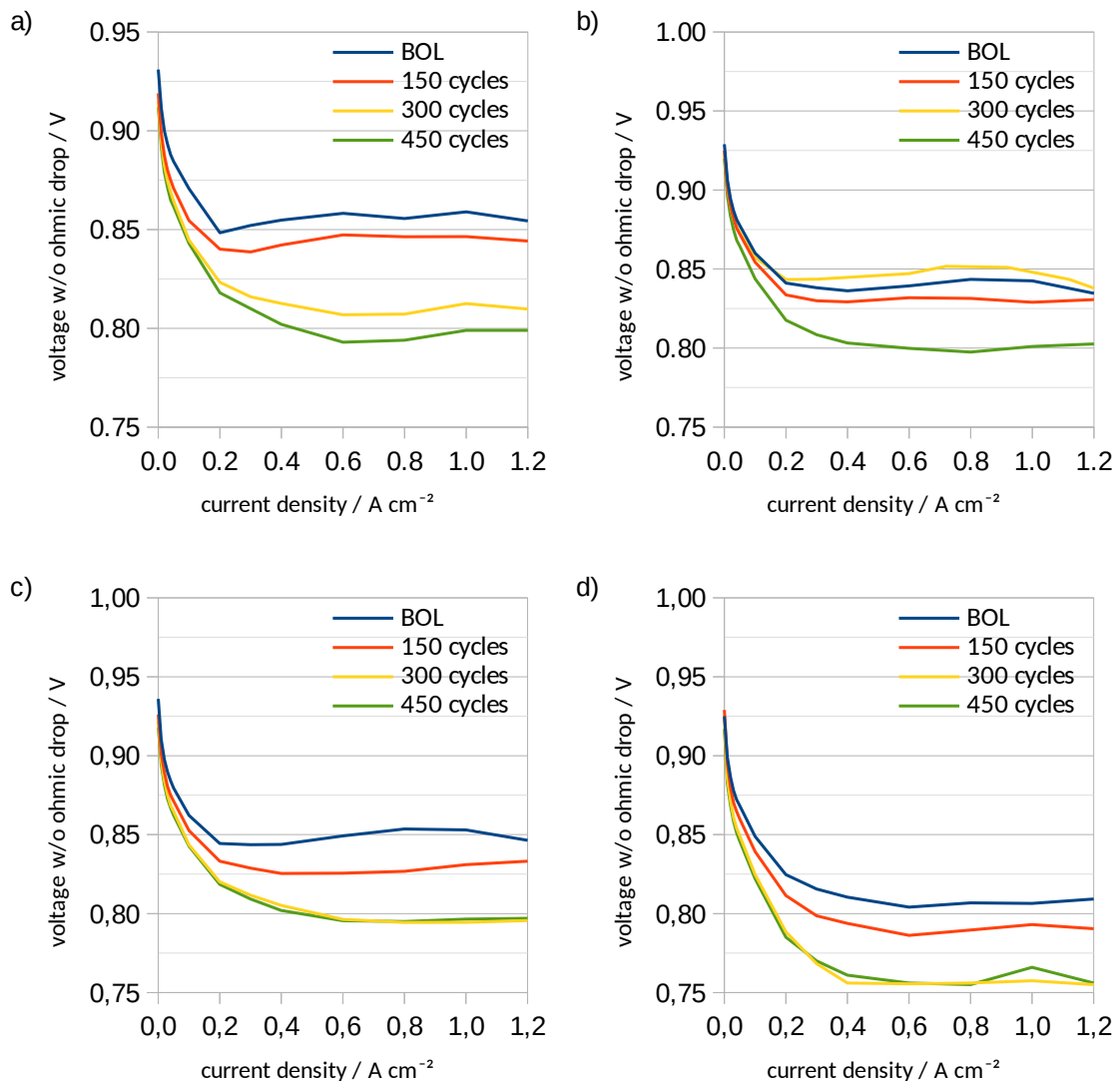
Figure 31: Corrected polarization curves without ohmic losses of a) SUSD strategy 1, b) SUSD strategy 2, c) SUSD strategy 3, and d) SUSD strategy 4

Table 3: Specific ohmic resistances calculated from the polarization curves of SUSD strategies 1-4

	specific ohmic resistance / mΩ cm^2			
cycles	SUSD 1	SUSD 2	SUSD 3	SUSD 4
0	247	231	228	229
150	275	243	216	242
300	227	322	226	228
450	250	228	232	280

The power curves presented in 32 give a better view of the influence on the diffusion controlled current density regions (1.2-2.0 A cm^{-2}). They show that the maximum power shifts towards higher current densities after SUSD strategies 1-3 are applied (32a-c). In contrast, anode air purge SUSD strategy 4 significantly diminishes maximum power and shifts the peak towards lower current densities, this correlates with performance decrease with increasing number of cycles. The losses of maximum power of SUSD 1-3 after 450 cycles is rather low in comparison to SUSD 4. Contrary to what had been expected, only SUSD strategy 4 results in a consequent decrease in maximum power density with increasing number of cycles. None of the other strategies has its maximum power peak at BOL. Whith SUSD strategy 1, 2 and 3, the highest power density peak is reached after 300 cycles, 450 cycles and 150 cycles respectively. As stated before, the significance of these results is rather questionable, as inappropriate conditioning times or humidity fluctuations may cause deviations at high current density. However, for practical applications, these high load conditions are less a point of interest, as long lasting operation under high currents and low voltages are harmful for the cell as well. At a moderate load of 1 A cm^{-2}, power clearly tends to decrease as the number of cycles grows. The power density values measured at 1 A cm^{-2} are shown in 4. Regarding these power losses, the OCV avoiding SUSD 2 shows the best results with a terminal loss of 5.1%, applying the load in steps leads to a slightly worse result, with 8.4% loss for SUSD 3, SUSD 1 loses 10,4% power, again anode air purging proves inferior, as it leads to a power loss of 15,9%.
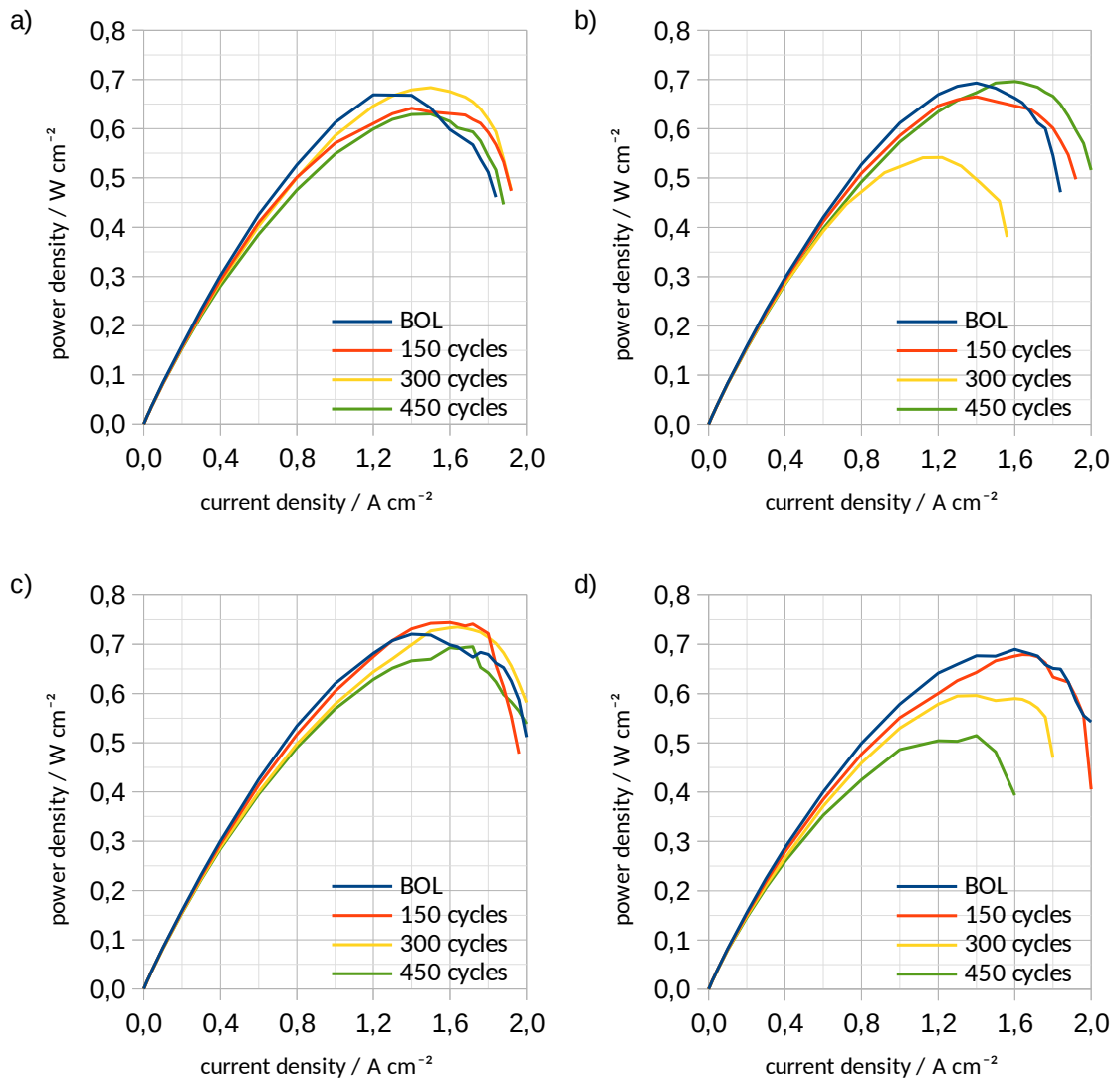
Figure 32: Power curves of a) SUSD strategy 1, b) SUSD strategy 2, c) SUSD strategy 3, and d) SUSD strategy 4

Table 4: Power densities at a current density of 1 A cm^{-2} during SUSD strategies 1-4 and total power density losses

cycles	Power density / W cm^{-2}			
	SUSD 1	SUSD 2	SUSD 3	SUSD 4
0	0.613	0.612	0.621	0.578
150	0.571	0.586	0.605	0.551
300	0.586	0.573	0.579	0.530
450	0.549	0.581	0.569	0.486
Δ0-450	**-0.064**	**-0.031**	**-0.052**	**-0.092**

4.3. Cyclic voltammetry

Like other results discussed previously in this chapter, cyclic voltammetry shows a similar pattern for SUSD strategies 1-3, being in a sharp contrast to the anode air purge variant. Of the cyclic voltammograms shown in 33, only the one belonging to SUSD 4 exhibits a typical pattern indicating loss of ECSA, since the area under the H_2 desorption peak decreases. This is a strong indication for carbon corrosion induced by the presence of H_2/O_2 boundaries during SUSD strategy 4. The calculated ECSA values resulting from all four SUSD strategies can be found in 5. The surface area reduces continuously with increasing number of cycles, after 450 cycles, the eventual loss is 34.7%. Noticeable for this strategy is the very low initial ECSA, significantly deviating from the BOL values determined for the CCMs used for the other SUSD strategies. As the performance of this cell is comparable to the others, which can be seen in the Figures 30 and 32, this CV result is very likely distorted by air leaking into the anode due to the modifications done to the test station for this SUSD strategy. However, these circumstances most probably only affect the absolute values and not the differences determined at different SUSD cycles.

None of SUSD strategies 1-3 has resulted in a decreased ECSA after 450 cycles, instead, all CV measurements done after cycling show higher surface areas than the BOL ones. SUSD 2 exhibits a continuous surface area growth through all cycling series, with SUSD 1 and 3 there is a turning point within the range of cycles covered by these experiments, after 450 cycles a degradation in ECSA can be observed for both strategies, however this degradation is very slightly in SUSD 1 and significantly higher in SUSD 3. It seems that carbon corrosion may initially increase the ECSA to a certain degree before performance degradation can be observed, this explanation is strengthened by partial increases in cell performance at high currents, as discussed previously.
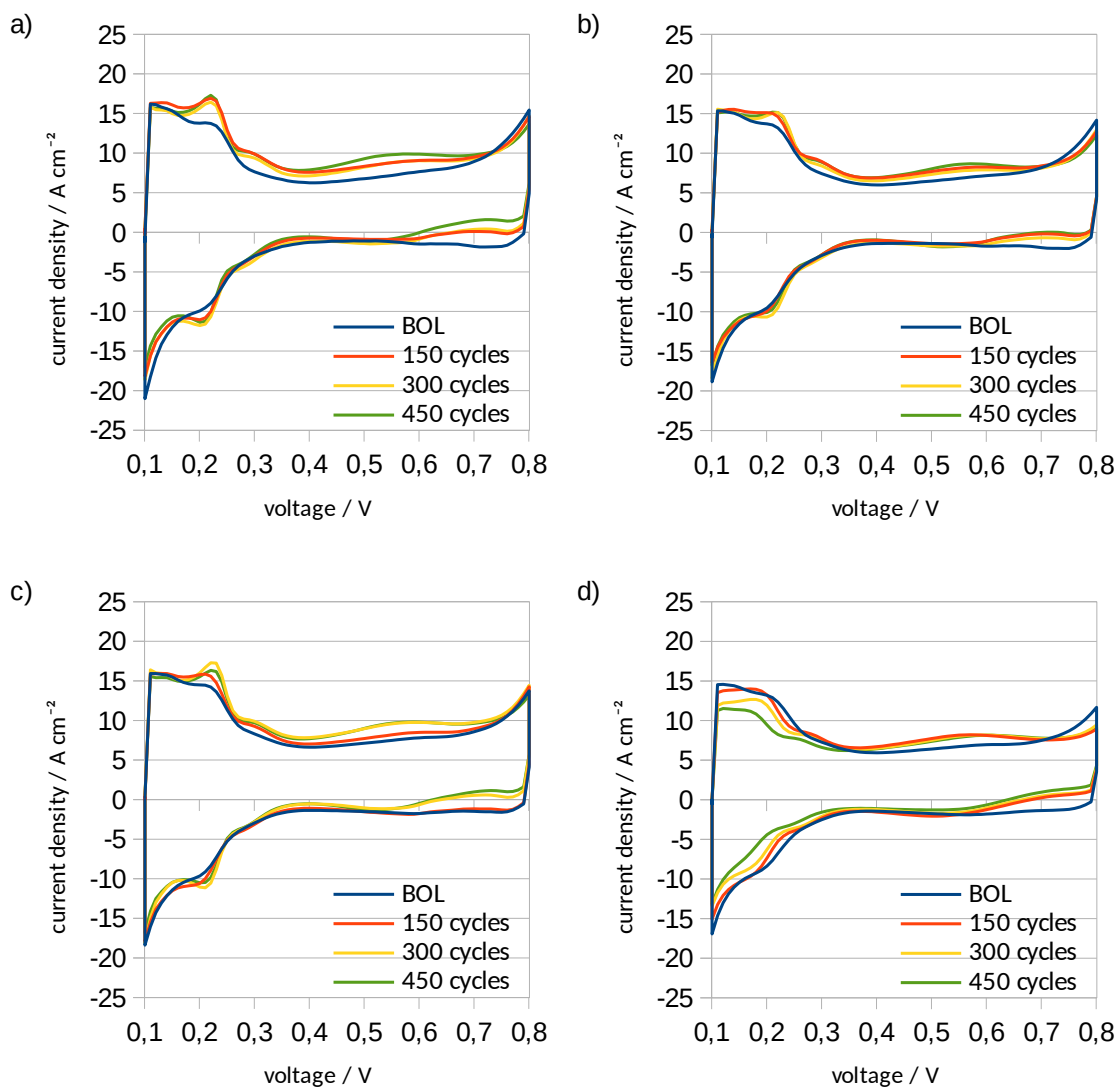
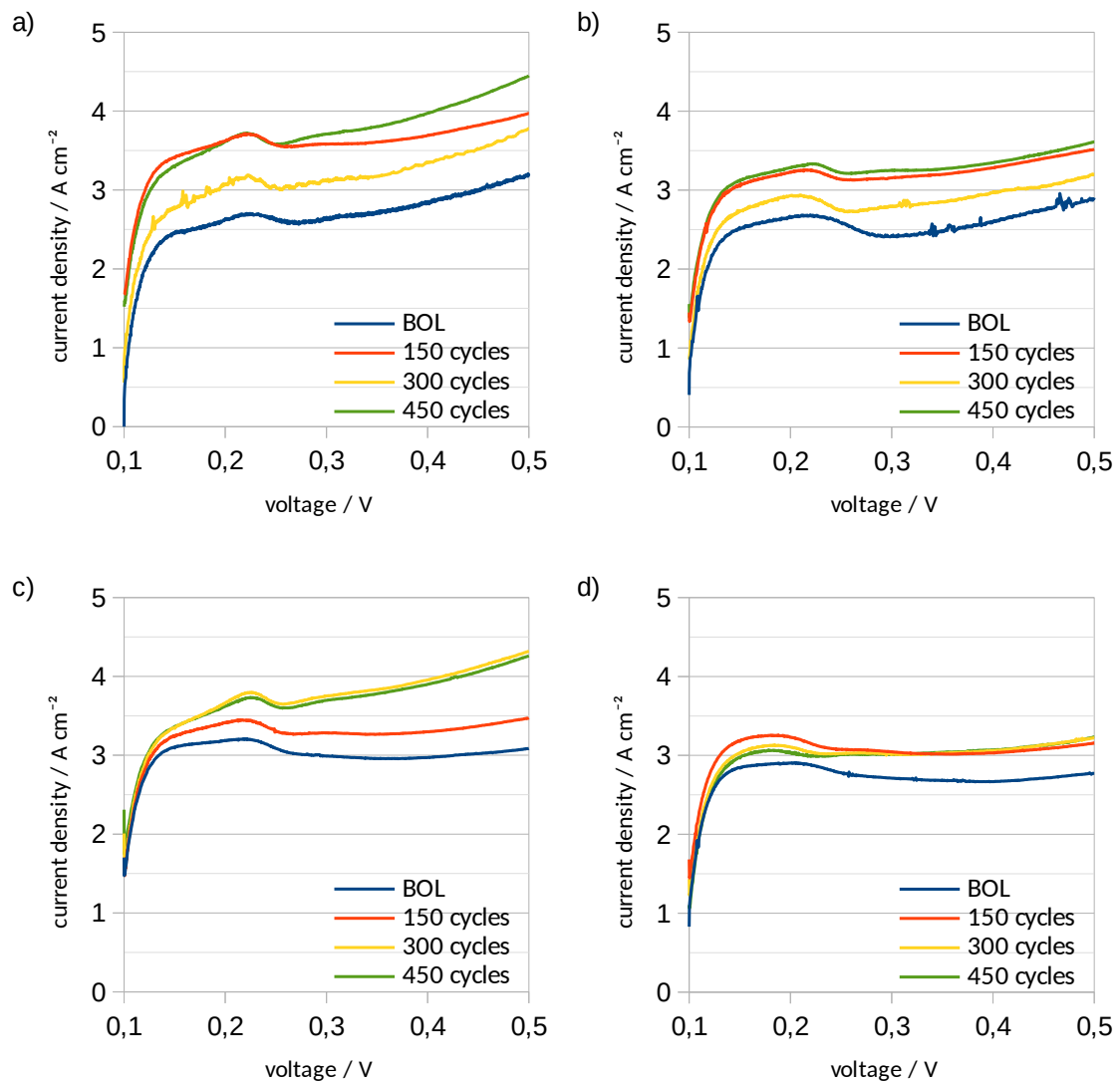*Figure 33: Cyclic voltammograms at BOL and after each 150 cycles of a) SUSD strategy 1, b) SUSD strategy 2, c) SUSD strategy 3, and d) SUSD strategy 4*

Table 5: ECSA calculated from CV data for SUSD strategies 1-4

cycles	ECSA / $m^2\ g^{-1}$			
	SUSD 1	**SUSD 2**	**SUSD 3**	**SUSD 4**
0	44.1	42.7	49.2	29.4
150	45.3	47.3	49.7	28.5
300	47.3	49.1	54.8	24.4
450	47.1	50.1	51.1	19.2
Δ0-450	**+3.0**	**+7.4**	**+1.9**	**-10.2**

4.4. Linear sweep voltammetry

The linear sweep voltammograms shown in 34 and the resulting H_2 crossover rates are listed in 6 clearly show that in all four SUSD strategies H_2 crossover increases, however for none of them a correlation between H_2 crossover rate and the amount of cycles can be observed. Also, the crossover varies between $1.39*10^{-8}\,mol\,cm^{-2}\,s^{-1}$ and $1.66*10^{-8}\,mol\,cm^{-2}\,s^{-1}$ within the different CCMs at BOL conditions. Considering this scattering and the apparent randomness of the results received from the measurements after cycling, one has to assume that the influence of SUSD cycling in this extent on the membrane is too small to draw quantitative conclusions from the LSV measuremtents. There are multiple possible reasons causing the deviations of the LSV measurements. As seen in 34, not only the H_2 crossover current peaks visible near 0.2 V vary significantly within the same strategy, but also the slope of the graph above 0.3 V does as well. This indicates different internal short currents, hence the electrical resistance of the electrolyte membrane also changes. These changes could be a result of fluctuations of the gas humidities. Another reason might be the impact of OCV related degradation, such as damage done by H_2O_2, which are partially reversible, as discussed in the theory section (see chapter 2.4).

Figure 34: Linear sweep voltammograms at begin of life and after each 150 cycles of of a) SUSD strategy 1, b) SUSD strategy 2, c) SUSD strategy 3, and d) SUSD strategy 4

Table 6: H_2 crossover rates calculated from LSV data of SUSD strategies 1-4

cycles	H_2 crossover rate / mol cm^{-2} s^{-1}			
	SUSD 1	**SUSD 2**	**SUSD 3**	**SUSD 4**
0	$1.40*10^{-8}$	$1.39*10^{-8}$	$1.66*10^{-8}$	$1.51*10^{-8}$
150	$1.93*10^{-8}$	$1.69*10^{-8}$	$1.79*10^{-8}$	$1.69*10^{-8}$
300	$1.65*10^{-8}$	$1.52*10^{-8}$	$1.97*10^{-8}$	$1.62*10^{-8}$
450	$1.93*10^{-8}$	$1.73*10^{-8}$	$1.94*10^{-8}$	$1.59*10^{-8}$

4.5. Electrochemical impedance spectroscopy

The data received from EIS is presented as Nyquist plot and can be seen in 35. Looking at the shape of the curves, for neither of the tested strategies a trend can be discovered. The high frequency resistances, which can be found in 7, do not show any correlation with the number of SUSD cycles as well. Except for SUSD 3, where there is a relatively high scattering within the values, the resistances seem not to change significantly after SUSD cycling.

Comparable experiments, e.g. those carried out by Lin et al. indeed show a trend regarding impedance. Both the real and the imaginary parts increase with the number of cycles. However in these experiments a total of 1800 SUSD cycles were applied and characterization was done after every 300 cycles. The measured high frequency resistance measured at BOL is 85 mΩ cm^2, after 1800 cycles it increased to 115.5 mΩ cm^2. [41]

Hence the most likely reason why no trend can be observed in the EIS results of SUSD strategies 1-4 is that the observation range is insufficiently small. Within only several hundreds of cycles, the influences of other factors such as temperature and humidity fluctuations seems to be higher than those of the changes caused by SUSD.

Table 7: High frequency restistance values calculated from EIS data

	High frequency resistance / mΩ cm^2			
cycles	**SUSD 1**	**SUSD 2**	**SUSD 3**	**SUSD 4**
0	58.3	55.3	57.7	61.1
150	59.4	56.5	49.0	61.2
300	53.5	55.6	65.5	82.4
450	58.3	57.9	83.6	61.3
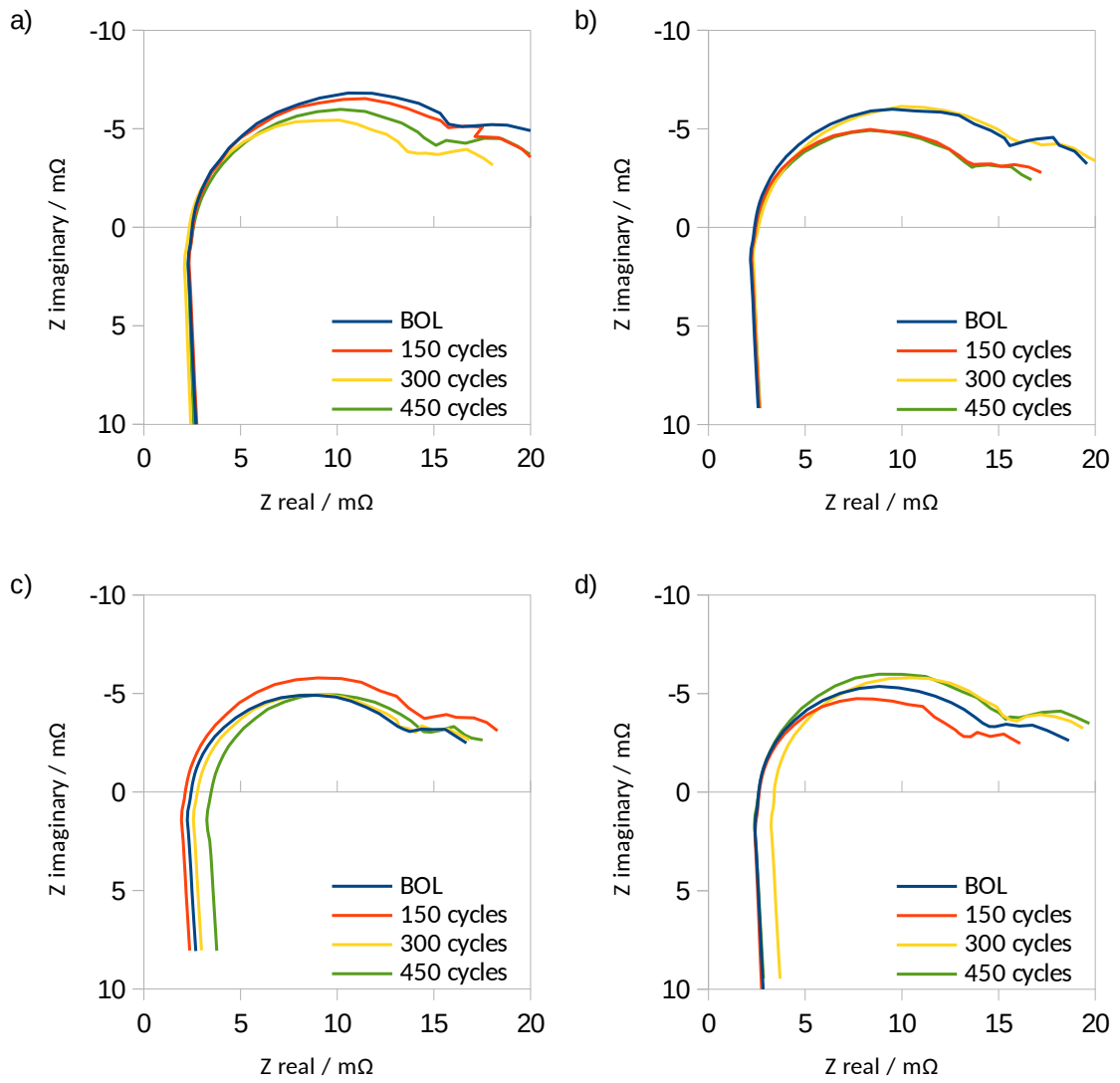
Figure 35: EIS results presented as Nyquist plots at begin of life and after each 150 cycles of of a) SUSD strategy 1, b) SUSD strategy 2, c) SUSD strategy 3, and d) SUSD strategy 4

4.6. Exhaust gas measurements

Regarding carbon corrosion, the exhaust gas analysis results show a huge difference between SUSD strategies 1-3 and SUSD strategy 4. While the CO levels are below the limit of detection (<0.1 ppm) in all tested SUSD strategies, significant amounts of CO_2 are produced in each strategy. The measured CO_2 concentration peaks have been integrated to calculate the absolute amounts of CO_2 formed with each strategy. As shown in 36, the average mass of CO_2 released at the cathode during a single cycle of SUSD 4 (13.9 µg, or $3.16*10^{-7}$ mol) is roughly 3-4 times higher, compared to the other strategies.
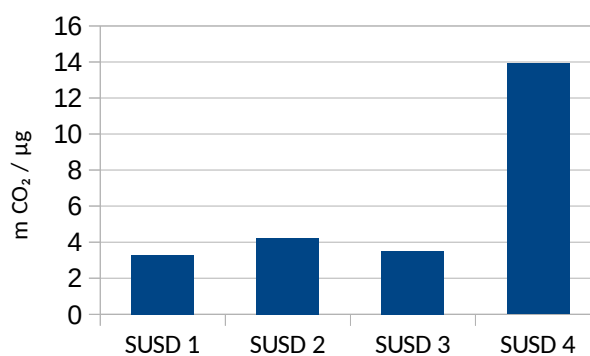
Figure 36: Average amount of CO_2 formed at the cathode per cycle of SUSD 1-4

37 shows that the vast majority of the CO_2 produced during SUSD 4 is formed right after H_2 is introduced into the air filled anode. As expected and explained in the theory (see chapter 2.4), the biggest share of PEFC degradation is a result of carbon corrosion caused by the high potentials occurring due to the H_2/O_2 boundaries. However, the CO_2 peak measured during shutdown is extremely small, if compared to the one during startup. Probably, this is a result of the different gas flow rates at the anode. When H_2 is turned on during startup, it is introduced into the anode at 0.2 NLPM, whereas the air purge during shutdown is done at 0.5 NLPM. The H_2/O_2 boundary formed during startup moves slower and stays inside the cell for a longer time, thus more CO_2 is formed. As the air purge is faster, there is less CO_2 is produced, additionally the time while CO_2 enriched cathode off gas is present in the gas analyzer's detector is also shorter. During the gas measurement, one point per second is recorded, so possibly the CO_2 formed at shutdown passes the analyzer without being detected.

While the CO_2 peaks can be easily assigned to certain sections of the SUSD procedure for SUSD 4, this is not the case with the other three strategies, as the cathode gas flow is stopped during the shutdown sequence. CO_2 possibly formed during shutdown is accumulated and detected when the cathode gas is turned on again, overlapping with the startup. However, assumptions can be made after comparing the results of SUSD strategies 1-3. Of those, SUSD 1 reveals the smallest amount of CO_2 emission with 3.28 µg ($7.45*10^{-8}$ mol) per cycle. SUSD 3 is slighly above, with 3.53 µg ($8.01*10^{-8}$ mol). This is most likely because the cell was exposed to higher voltage conditions for a longer time. This was tried to avoid with SUSD 2, however, with 4.23 µg ($9.61*10^{-8}$ mol) per cycle it shows the highest amount of CO_2 emission among the O_2 consumption SUSD strategies. The most likely explanation for this might be that the early application of an electric load to prevent OCV causes increased hydrogen starvation, probably nullifying the benefit of this strategy.
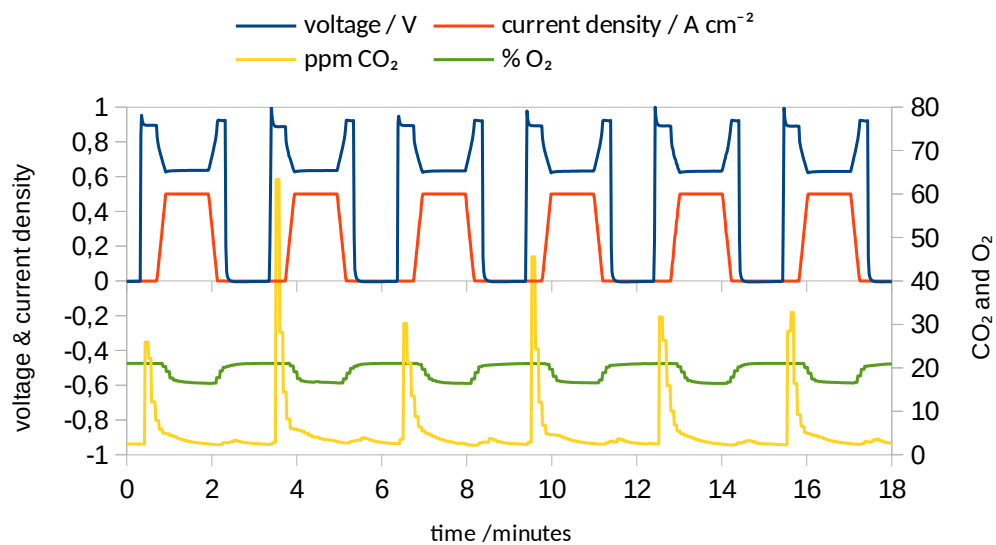
Figure 37: CO_2 and O_2 concentration in the cathode exhaust gas during SUSD 4

5. Conclusion

In this thesis, different startup and shutdown (SUSD) strategies for PEFCs were compared. The main target was to improve cell durability by avoiding the formation of H_2/O_2 boundaries at the anode, which are known to foster carbon corrosion, damaging the catalyst support and thus lead to significant performance decay. To achieve this target, an O_2 consumption SUSD strategy was chosen. In this strategy, during shutdown, the anode was kept under hydrogen atmosphere while the cathode air supply was turned off and the residual O_2 was reacted by applying a small current load, finally leading to an inert N_2 atmosphere at the cathode. As keeping PEFCs at OCV as well as H_2 starvation during startup are also known as sources of cell degradation, two more variations of this strategy were investigated to test whether cell lifetime could be further improved. Of these modified strategies, the first was set to keep voltage from reaching OCV with a potentiostatic load control. In the second strategy, the electric load was increased and decreased in stages to give the cell to minimize H_2 starvation effects. For comparison a fourth SUSD strategy was tested, in which a H_2/O_2 boundary is simulated by purging the anode with air during shutdown. Of each strategy, 450 SUSD cycles were applied, the cell was characterized by recording polarisation curves as well as using CV, LSV and EIS. To quantify carbon corrosion, the CO_2 and CO contents in the cathode off gas were measured.

The results clearly show that avoiding H_2/O_2 boundaries during SUSD mitigates PEFC degradation effects. All of three O_2 consumption strategies caused less performance degradation, compared to the anode air purge strategy. Regarding loss of power and CO_2 formation (carbon corrosion), the standard O_2 consumption SUSD strategy tested first led to the best results. While still resulting in less performance loss than the anode air purge strategy, neither the OCV avoiding SUSD strategy nor the H_2 starvation mitigation SUSD strategy proved to be an improvement of the first strategy. In contrast to their initial purpose, these variants exhibited even more performance loss as well as higher CO_2 emissions. For further investigation of the processes taking place inside the cell during SUSD, current distribution measurements will probably give more detailed information. Therefore the use of a segmented sensor plate capable of

spatially resolving the current density would be beneficial.

According to the CV results, the presence of H_2/O_2 boundaries seem to be a root cause for ECSA detoriation, as only the fourth SUSD strategy led to an observable reduction of ECSA. The other strategies have shown no sign of decreasing surface area. Instead, for all of them the ECSA determined after 450 cycles was even larger than at the begin of life (BOL) state. No conclusions regarding impacts of SUSD could be drawn from both LSV and EIS measurements. While increased H_2 crossover was observed after 450 cycles of each SUSD strategy, no correlations to the specific strategy or to the number of cycles could be found. SUSD cycling also seemed to have no effect on the recorded impedance spectra. It is assumed that regeneration effects have a significant impact on these results, as electrolyte membrane degradation is known to be reversible to some extend. Therefor, further research to quantify the reversibility of PEFC degradation effects is advised. Overall the difference of the results of the different SUSD strategies is rather small, especially among the three O_2 strategies. In order to receive more significant data, future SUSD experiments should be done in a wider range by extensive expansion of the number of SUSD cycles to several thousands rather than several hundreds.

Another possible source of uncertainties are fluctuations of operating conditions, such as cell temperature and especially the relative humidity of the reactant gases. For a better control of gas RH, the implementation of humidity sensors close to the cell outlets would be advantageous, since indirect RH control via dewpoint temperatures is often too inaccurate in practical application.

6.   References

[1]   N. Zhou, "Oxford Dictionaries declares 'climate emergency' the word of 2019," *The Guardian*, Nov. 21, 2019.

[2]   "The Paris Agreement | UNFCCC." https://unfccc.int/process-and-meetings/the-paris-agreement/the-paris-agreement (accessed Nov. 21, 2019).

[3]   A. Mahmoudzadeh Andwari, A. Pesiridis, S. Rajoo, R. Martinez-Botas, and V. Esfahanian, "A review of Battery Electric Vehicle technology and readiness levels," *Renew. Sustain. Energy Rev.*, vol. 78, pp. 414–430, Oct. 2017, doi: 10.1016/j.rser.2017.03.138.

[4]   P. Kurzweil, "Polymerelektrolyt-Brennstoffzelle," in *Brennstoffzellentechnik*, Wiesbaden: Springer Fachmedien Wiesbaden, 2016, pp. 77–144.

[5]   "Fuel Cell Technologies Office Multi-Year Research, Development, and Demonstration Plan Section 3.4," *US Department of Energy*, 2016. https://www.energy.gov/eere/fuelcells/downloads/fuel-cell-technologies-office-multi-year-research-development-and-22 (accessed Mar. 01, 2020).

[6]   R. P. O'Hayre, "Chapter 1: Introduction," in *Fuel Cell Fundamentals*, Hoboken, NJ, USA: John Wiley & Sons, Inc, 2016, pp. 1–24.

[7]   "PEM fuel cell - Datei:PEM fuel cell.svg – Wikipedia." https://commons.wikimedia.org/wiki/File:PEM_fuel_cell.svg (accessed Dec. 29, 2019).

[8]   F. Barbir, "Fuel Cell Basic Chemistry and Thermodynamics," in *PEM Fuel Cells*, Elsevier, 2013, pp. 17–32.

[9]   F. Barbir, "Fuel Cell Electrochemistry," in *PEM Fuel Cells*, Elsevier, 2013, pp. 33–72.

[10]   P. Kurzweil, "Thermodynamik und Kinetik der Brennstoffzelle," in *Brennstoffzellentechnik*, Wiesbaden: Springer Fachmedien Wiesbaden, 2016, pp. 17–52.

[11]   W. Shi and L. A. Baker, "Imaging heterogeneity and transport of degraded Nafion membranes," *RSC Adv.*, vol. 5, no. 120, pp. 99284–99290, 2015, doi: 10.1039/C5RA20291D.

[12]   F. Barbir, "Main Cell Components, Material Properties, and Processes," in *PEM Fuel Cells*, Elsevier, 2013, pp. 73–117.

[13]   X.-Z. Yuan, S. Zhang, J. C. Sun, and H. Wang, "A review of accelerated conditioning for a polymer electrolyte membrane fuel cell," *J. Power Sources*, vol. 196, no. 22, pp. 9097–9106, Nov. 2011, doi: 10.1016/j.jpowsour.2011.06.098.

[14]   H. C. Kang, K. M. Jum, and Y. J. Sohn, "Performance of unit PEM fuel cells with a leaf-vein-simulating flow field-patterned bipolar plate," *Int. J. Hydrog. Energy*, vol. 44, no. 43, pp. 24036–24042, Sep. 2019, doi: 10.1016/j.ijhydene.2019.07.120.

[15]   "H2Training: Technisch-pädagogischer Bereich." https://www.h2training.eu/tecnico_de.htm (accessed Jan. 15, 2020).

[16]   J. Tan, Y. J. Chao, M. Yang, C. T. Williams, and J. W. Van Zee, "Degradation Characteristics of Elastomeric Gasket Materials in a Simulated PEM Fuel Cell Environment," *J. Mater. Eng. Perform.*, vol. 17, no. 6, pp. 785–792, Dec. 2008, doi: 10.1007/s11665-008-9233-5.

[17]   R. P. O'Hayre, "Chapter 7: Fuel Cell Characterization," in *Fuel Cell Fundamentals*, Hoboken, NJ, USA: John Wiley & Sons, Inc, 2016, pp. 237–270.

[18]   J. Wu, X. Z. Yuan, H. Wang, M. Blanco, J. J. Martin, and J. Zhang, "Diagnostic tools in PEM fuel cell research: Part I Electrochemical techniques," *Int. J. Hydrog. Energy*, vol. 33, no. 6, pp. 1735–1746, Mar. 2008, doi:

10.1016/j.ijhydene.2008.01.013.

[19] V. Hacker, K. Mayer, and K. Kocher, "Fuel Cells," presented at the Laboratory Course Technical Chemistry II, Graz University of Technology, 2019, Accessed: Jan. 21, 2020. [Online]. Available: https://online.tugraz.at/tug_online/ee/ui/ca2/app/desktop/#/slc.tm.cp/student/courses/224158?$ctx=design=ca;lang=de;profile=STUDENT;rbacId=.

[20] R. P. O'Hayre, "Fuel cells for electrochemical energy conversion," *EPJ Web Conf.*, vol. 148, p. 00013, 2017, doi: 10.1051/epjconf/201714800013.

[21] H. Wang, "Fuel Cell Diagnostics," in *PEM Fuel Cells*, Elsevier, 2013, pp. 265–304.

[22] S. WASTERLAIN *et al.*, "Study of temperature, air dew point temperature and reactant flow effects on PEFC performances using electrochemical spectroscopy and voltammetry techniques," *J. Power Sources*, vol. 195, no. 4, pp. 984–993, Jan. 2010, doi: 10.1016/j.jpowsour.2009.08.084.

[23] A. J. L. Verhage, J. F. Coolegem, M. J. J. Mulder, M. H. Yildirim, and F. A. de Bruijn, "30,000 h operation of a 70 kW stationary PEM fuel cell system using hydrogen from a chlorine factory," *Int. J. Hydrog. Energy*, vol. 38, no. 11, pp. 4714–4724, Apr. 2013, doi: 10.1016/j.ijhydene.2013.01.152.

[24] P. Pei, Q. Chang, and T. Tang, "A quick evaluating method for automotive fuel cell lifetime," *Int. J. Hydrog. Energy*, vol. 33, no. 14, pp. 3829–3836, Jul. 2008, doi: 10.1016/j.ijhydene.2008.04.048.

[25] A. Oyarce *et al.*, "Comparing shut-down strategies for proton exchange membrane fuel cells," *J. Power Sources*, vol. 254, pp. 232–240, May 2014, doi: 10.1016/j.jpowsour.2013.12.058.

[26] C. A. Reiser *et al.*, "A Reverse-Current Decay Mechanism for Fuel Cells," *Electrochem. Solid-State Lett.*, vol. 8, no. 6, p. A273, 2005, doi: 10.1149/1.1896466.

[27] H. Tang, Z. Qi, M. Ramani, and J. F. Elter, "PEM fuel cell cathode carbon corrosion due to the formation of air/fuel boundary at the anode," *J. Power Sources*, vol. 158, no. 2, pp. 1306–1312, Aug. 2006, doi: 10.1016/j.jpowsour.2005.10.059.

[28] N. Yousfi-Steiner, Ph. Moçotéguy, D. Candusso, and D. Hissel, "A review on polymer electrolyte membrane fuel cell catalyst degradation and starvation issues: Causes, consequences and diagnostic for mitigation," *J. Power Sources*, vol. 194, no. 1, pp. 130–145, Oct. 2009, doi: 10.1016/j.jpowsour.2009.03.060.

[29] K. H. Lim, H.-S. Oh, S.-E. Jang, Y.-J. Ko, H.-J. Kim, and H. Kim, "Effect of operating conditions on carbon corrosion in polymer electrolyte membrane fuel cells," *J. Power Sources*, vol. 193, no. 2, pp. 575–579, Sep. 2009, doi: 10.1016/j.jpowsour.2009.04.006.

[30] J. Kim, J. Lee, and Y. Tak, "Relationship between carbon corrosion and positive electrode potential in a proton-exchange membrane fuel cell during start/stop operation," *J. Power Sources*, vol. 192, no. 2, pp. 674–678, Jul. 2009, doi: 10.1016/j.jpowsour.2009.03.039.

[31] K. Teranishi, K. Kawata, S. Tsushima, and S. Hirai, "Degradation Mechanism of PEFC under Open Circuit Operation," *Electrochem. Solid State Lett.*, vol. 9, no. 10, p. A475, Aug. 2006, doi: 10.1149/1.2266163.

[32] N. Ramaswamy, N. Hakim, and S. Mukerjee, "Degradation mechanism study of perfluorinated proton exchange membrane under fuel cell operating conditions," *Electrochimica Acta*, vol. 53, no. 8, pp. 3279–3295, Mar. 2008, doi: 10.1016/j.electacta.2007.11.010.

[33] K. Ono, Y. Yasuda, K. Sekizawa, N. Takeuchi, T. Yoshida, and M. Sudoh, "Evaluation of Pt/C catalyst degradation and H2O2 formation changes under simulated PEM fuel cell condition by a rotating ring-disk electrode," *Electrochimica Acta*, vol. 97, pp. 58–65, May 2013, doi: 10.1016/j.electacta.2013.02.070.

[34] K. Hongsirikarn, X. Mo, J. G. Goodwin, and S. Creager, "Effect of H2O2 on Nafion® properties and conductivity at fuel cell conditions," *J. Power Sources*, vol. 196, no. 6, pp. 3060–3072, Mar. 2011, doi: 10.1016/j.jpowsour.2010.11.133.

[35] S. Kundu, M. Fowler, L. C. Simon, and R. Abouatallah, "Reversible and irreversible degradation in fuel cells during Open Circuit Voltage durability testing," *J. Power Sources*, vol. 182, no. 1, pp. 254–258, Jul. 2008, doi: 10.1016/j.jpowsour.2008.04.009.

[36] P. Gazdzicki, J. Mitzel, D. Garcia Sanchez, M. Schulze, and K. A. Friedrich, "Evaluation of reversible and irreversible degradation rates of polymer electrolyte membrane fuel cells tested in automotive conditions," *J. Power Sources*, vol. 327, pp. 86–95, Sep. 2016, doi: 10.1016/j.jpowsour.2016.07.049.

[37] T. Zhang, P. Wang, H. Chen, and P. Pei, "A review of automotive proton exchange membrane fuel cell degradation under start-stop operating condition," *Appl. Energy*, vol. 223, pp. 249–262, Aug. 2018, doi: 10.1016/j.apenergy.2018.04.049.

[38] R. Lin, B. Li, Y. P. Hou, and J. M. Ma, "Investigation of dynamic driving cycle effect on performance degradation and micro-structure change of PEM fuel cell," *Int. J. Hydrog. Energy*, vol. 34, no. 5, pp. 2369–2376, Mar. 2009, doi: 10.1016/j.ijhydene.2008.10.054.

[39] "Freudenberg H14C7." https://www.fuelcellstore.com/freudenberg-h1410-i2-c7 (accessed Apr. 15, 2020).

[40] D. Bezmalinović, J. Radošević, and F. Barbir, "Initial conditioning of Polymer Eelectrolyte Membrane fuel cell by temperature and potential cycling," *Acta Chim. Slov.*, vol. 62, no. 1, Mar. 2015, doi: 10.17344/acsi.2014.730.

[41] R. Lin, X. Cui, J. Shan, L. Técher, F. Xiong, and Q. Zhang, "Investigating the effect of start-up and shut-down cycles on the performance of the proton exchange membrane fuel cell by segmented cell technology," *Int. J. Hydrog. Energy*, vol. 40, no. 43, pp. 14952–14962, Nov. 2015, doi: 10.1016/j.ijhydene.2015.09.042.

7.   Abbreviations

AC	alternating current
BEV	battery electric vehicle
BOL	begin of life
CCM	catalyst coated membrane
CCU	cell compression unit
CV	cyclic voltammetry
DC	direct current
DP	dewpoint
EIS	electrochemical impedance spectroscopy
EV	electric vehicle
FC	fuel cell
FCEV	fuel cell electric vehicle
GDL	gas diffusion layer
GHG	greenhouse gas
HHV	higher heating value
HOR	hydrogen oxydation reaction
ICEV	internal combustion engine vehicle
j	current density
LHV	lower heating value
LSV	linear sweep voltammetry
OCV	open circuit voltage
ORR	oxygen reduction reaction
p	pressure
PEFC	polymer electrolyte membrane fuel cell
RH	relative humidity
SUSD	startup and shutdown
T	temperature
V	voltage
ΔG	Gibbs free enthalpy
ΔH	reaction enthalpy
ΔS	entropy change

8. List of Figures

Table of Figures

9.   List of Tables

Index of Tables